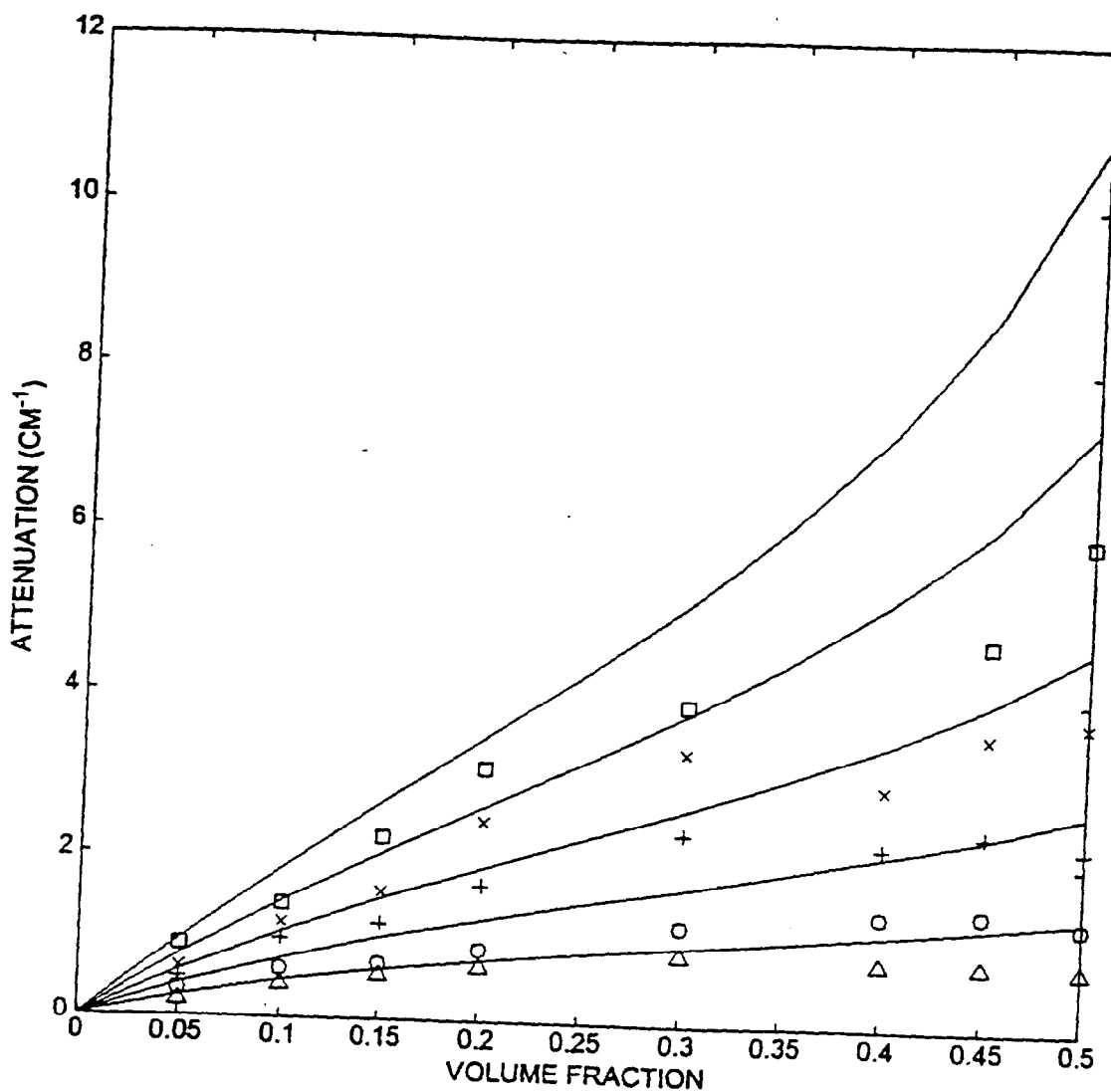


experimental data at these lower frequencies for solids volume fractions up to approximately 0.30.

The theory predictions begin to deviate more from the experimental data as the frequency increases. Figure 6.3 shows the experimental attenuation as a function of solids volume fraction in the Potter's Beads slurries for the relatively higher frequencies (3, 3.5, 4, 4.5 and 5 MHz), along with the corresponding effective medium theory predicted attenuation curves. The experimental data and theory prediction for 3 MHz show fairly good agreement up to a solids volume fraction of approximately 0.4. Otherwise for higher frequencies, the deviation between data and theory becomes noticeable at solids volume fractions greater than about 0.2. It should, again, be noted here that the experimental attenuation data display a local minimum between solids volume fractions of 0.35 and 0.5. And again, these local minima are not predicted by the effective medium theory. The deviation at the higher volume fraction and higher frequencies could also be attributed to the increased scatter in the attenuation data at the higher solids volume fractions, and the attenuation is especially large (implying small received voltage signals) for the higher frequencies at these higher solids volume fractions.

A more encouraging look into the efficacy of the effective medium approach can be achieved when the theoretical results are compared with other experimental data. For example, Figure 6.4 shows results of the effective medium approach (solid curves) compared with the experimental attenuation data (markers) of Allegra and Hawley (1972), which are for 0.11  $\mu\text{m}$  radius polystyrene particles in water at 3, 9, 15, 21, 27,



**Figure 6.3:** Attenuation as a function of solids volume fraction at various frequencies in slurries of Potter's beads in glycerin/water. Data are shown for 3.0 MHz ( $\Delta$ ); 3.5 MHz (O); 4.0 MHz (+); 4.5 MHz ( $\times$ ); and 5.0 MHz ( $\square$ ). The solid curves represent the results of the effective medium calculations using a particle size distribution with 65  $\mu\text{m}$  mean radius and standard deviation of 11  $\mu\text{m}$ . - E6173.

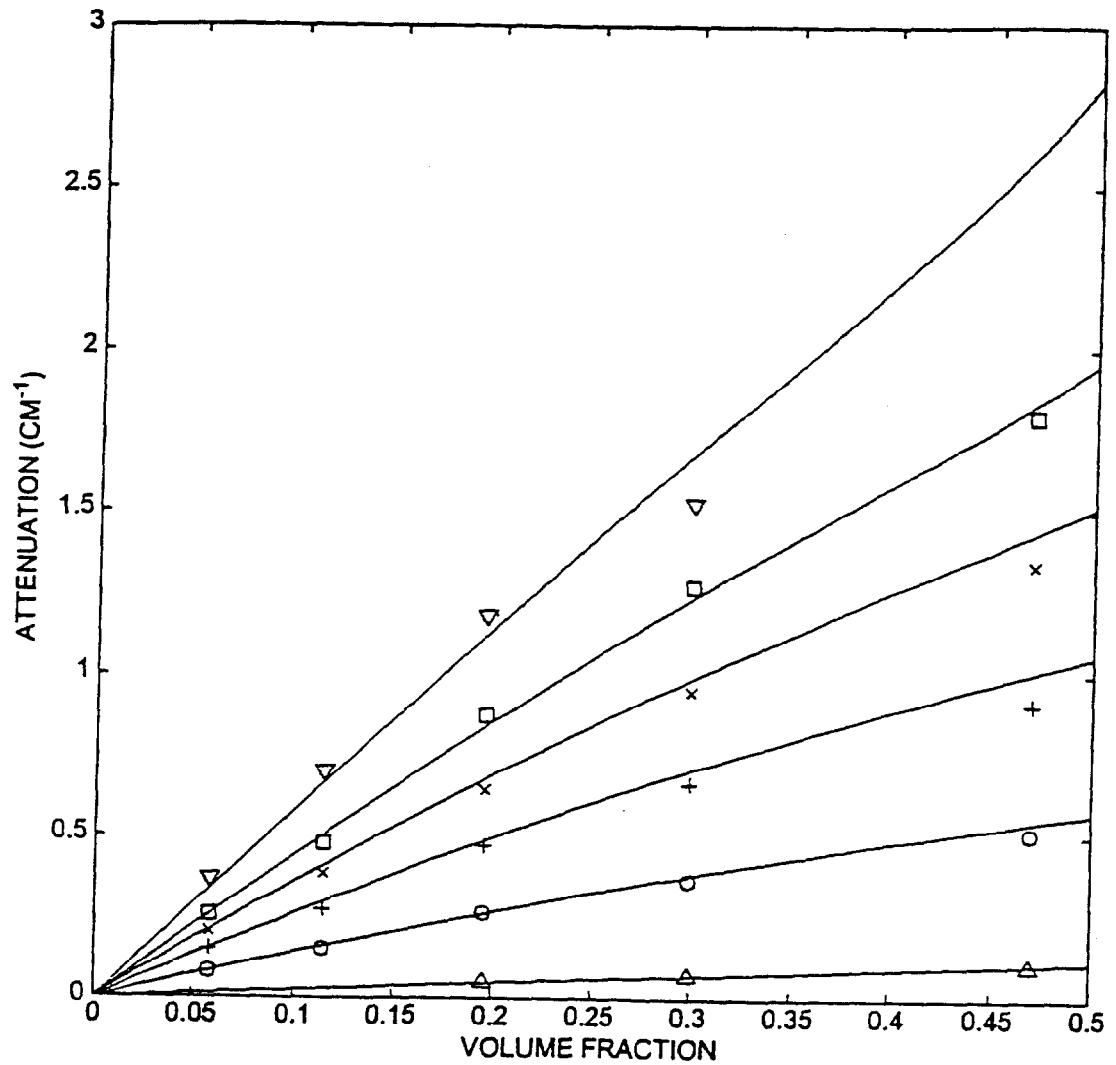


**Figure 6.4:** Attenuation as a function of solids volume fraction for the data of Allegra and Hawley (1972). The symbols represent experimental data at 3MHz ( $\Delta$ ); 9MHz (O); 15MHz (+); 21MHz ( $\times$ ); 27MHz ( $\square$ ); and 39 MHz ( $\nabla$ ). The solid curves represent the results of the effective medium approach used in this study.

and 39 MHz. For these systems, the agreement between the experimental data and theory is rather good for all solids volume fractions over the range which attenuation data are available for frequencies up to 27 MHz. Even at 39 MHz, the agreement between the experimental data and theory is fairly good up to a solids volume fraction of approximately 0.2.

Based on the results shown in Figure 6.4, the effective medium theory appears to describe the attenuation behavior as a function of solids volume fraction quite well, or at least when the particles are small and are of an elastic material like polystyrene. It is not clear as to why the results for the Potter's Beads slurries were not as good as for the slurry investigated by Allegra and Hawley (1972). It should be noted that the Potter's particles are soda-lime glass and they are, on average almost three orders of magnitude larger than the particles used by Allegra and Hawley (1972). The differences between the results for the two sets of data could be attributed to a behavior dependence based upon the different, particle size governed, attenuation regimes as was seen in the attenuation versus frequency curves.

## **Chapter 7: Theory and Experiments for Solid-Gas-Liquid Slurries**

### **7.1 Theory for the Effective Wavenumber in Solid-Gas-Liquid Slurries**

The theory developed in the previous chapter can be readily extended to treat suspensions having more than one species, e.g., solid particles and gas bubbles, and particles of different sizes. In this chapter we compare the predictions of the theory to experiments in solid-gas-liquid systems.

### **7.2 Attenuation Measurements in Solid-Gas-Liquid Slurries:**

Measurements of attenuation as a function of frequency were performed in solid-gas-liquid systems at low gas volume fraction. The first systems investigated were comprised of soda-lime glass spheres (as described in Section 3.2.1) in water at 5 % and 10 % by volume. The gas phase bubbles were produced first by electrolysis and then by sparging air at 150 ml/hr through a limewood aerator (as described in Section 3.3). The results of these attenuation measurements are shown in Figures 7.1 and 7.2. In these figures, the solid-liquid data are shown on the same plot as the solid-gas-liquid data for comparison. It should be noted that the gas phase volume fraction in the solid-gas-liquid systems is fairly small. In fact, the gas volume fraction is estimated, by use of the photomicrographic imaging system, at approximately 0.02 for the systems where the bubbles were generated by the limewood aerator and at approximately 0.002 for the

systems where the bubbles were generated by electrolysis (and in both cases are found to be overestimates based on comparison with forward theory predictions “fitted” to the experimental data). Therefore, addition of the gas phase has little effect on the solids volume fraction; and it can be assumed that the solids concentration remains essentially constant between the solid-liquid and solid-gas-liquid systems.

Figure 7.1 shows the attenuation versus frequency results for bubbles generated by the limewood aerator operating at a gas flow rate of 150 ml/hr. Comparing the curves for the solid-gas-liquid systems with those of the solid-liquid systems at the same solids concentration, the effect of the gas phase, even at these low concentrations, is quite apparent. The attenuation for the solid-gas-liquid slurries is essentially constant up to about 3 MHz, where the total attenuation is dominated by the contribution of the gas bubbles. Then, at higher frequencies, the attenuation begins to increase fairly rapidly as it becomes dominated by the attenuation due to the scattering regime for the solids. In fact, above approximately 6 MHz, the attenuation behavior is completely controlled by the attenuation due to the solid particles. This behavior is not surprising as the aerator generated bubbles are estimated to have a mean diameter of approximately 141  $\mu\text{m}$ , and bubbles of this size resonate at about 0.046 MHz (46 kHz). This resonance frequency is well below the range of frequencies investigated in this experimental study. Therefore, the contribution to the total attenuation by the bubbles is expected to be fairly small, and, the total attenuation in this region should be dominated by the solids. Whether or not the true bubble diameter is actually 141  $\mu\text{m}$  is not really relevant to the three phase behavior in this tail region. As long as the bubble size is such that the resonance frequency is

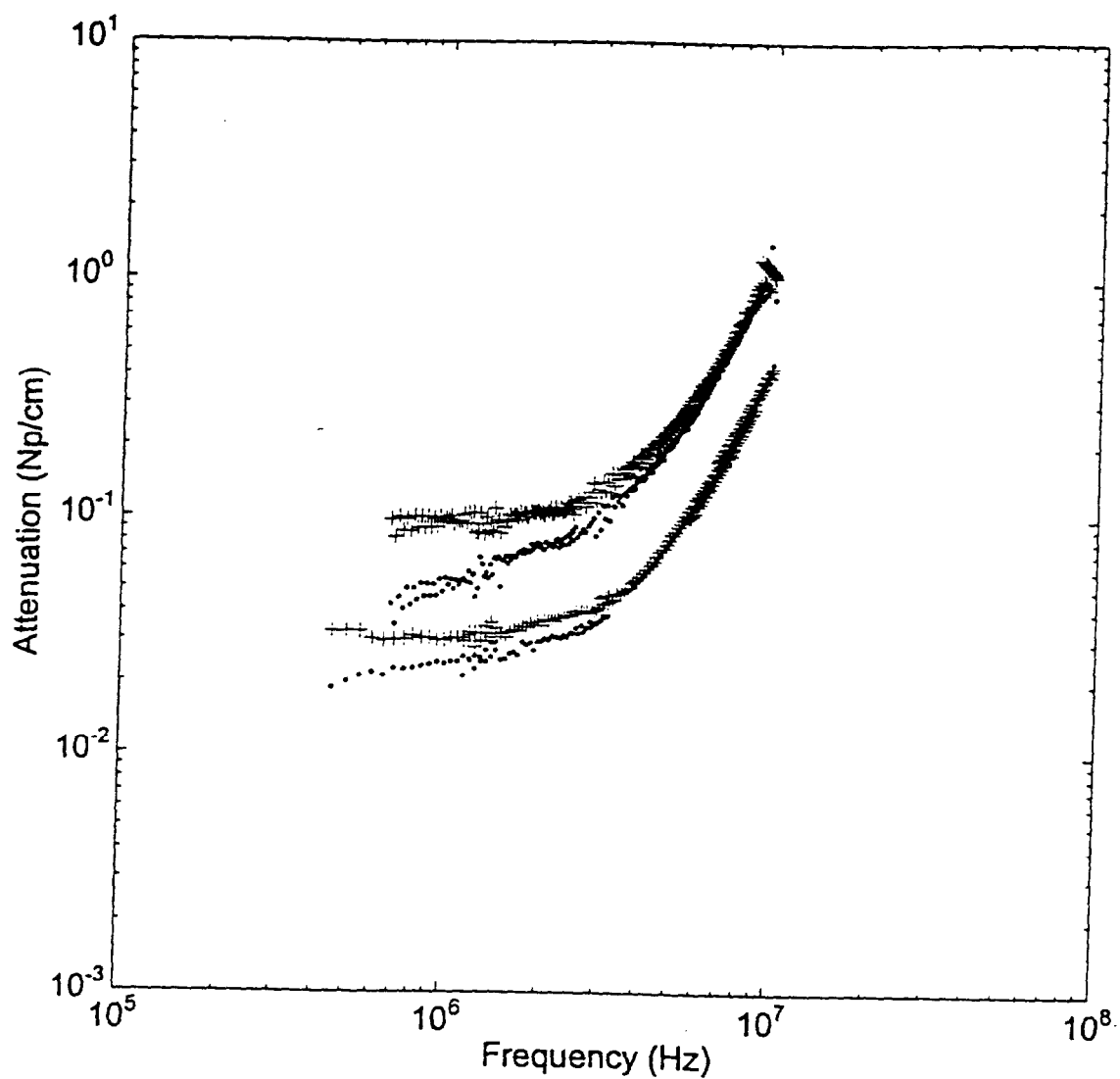


**Figure 7.1:** Attenuation versus frequency data for solid-gas-liquid systems of soda-lime glass beads in water at 5 % (lower curve) and 10 % solids by volume with bubbles generated by a limewood aerator with air flow rate of 150 ml/hr. The solid-gas-liquid data (+) are shown with solid-liquid data (•) at the same solids concentrations. The solids size distribution has a mean radius of 14.9  $\mu\text{m}$  with standard deviation of 3.56  $\mu\text{m}$ . - E2231.

below 0.1 MHz, the solid-gas-liquid data should behave in the manner shown in Figure 7.1. A resonance frequency of 0.1 MHz implies a bubble diameter of approximately 65  $\mu\text{m}$ , which is less than one half of the reported value from the photomicrographic bubble measurements. The photomicrographic technique does not, however, overestimate the bubble diameter by a factor of two. Therefore, in this context it is adequate to use the reported bubble diameter as a basis to interpret the solid-gas-liquid slurry behavior.

The influence of bubble size on the behavior of the solid-gas-liquid systems can be seen when the results in Figure 7.1 are compared with those shown in Figure 7.2. Figure 7.2 shows the attenuation spectra for the same soda-lime glass slurries as were shown in Figure 7.1. However, in this case, the bubbles for the solid-gas-liquid slurries were generated by electrolysis rather than by the aerator. Bubbles generated by electrolysis tend to have a smaller mean diameter (as described in Section 3.3), and this smaller diameter has an effect on the solid-gas-liquid attenuation results. In Figure 7.2 the attenuation for the solid-gas-liquid slurries is considerably higher in the 0.5 MHz to 1 MHz region than it is for the solid-gas-liquid slurries shown in Figure 7.1. Also, the attenuation for the solid-gas-liquid slurries in Figure 7.2 is never constant as in Figure 7.1. The reason for this difference is the considerably smaller mean diameter of the bubbles in the solid-gas-liquid slurries in Figure 7.2. The electrolytically generated bubbles, with a mean diameter of 51  $\mu\text{m}$ , have a resonance frequency of approximately 0.13 MHz. This frequency is much closer to (but still outside) the frequency range of investigation of these experiments. Therefore, the frequency range is such that the resonance peak has not completely decayed away to the constant attenuation behavior

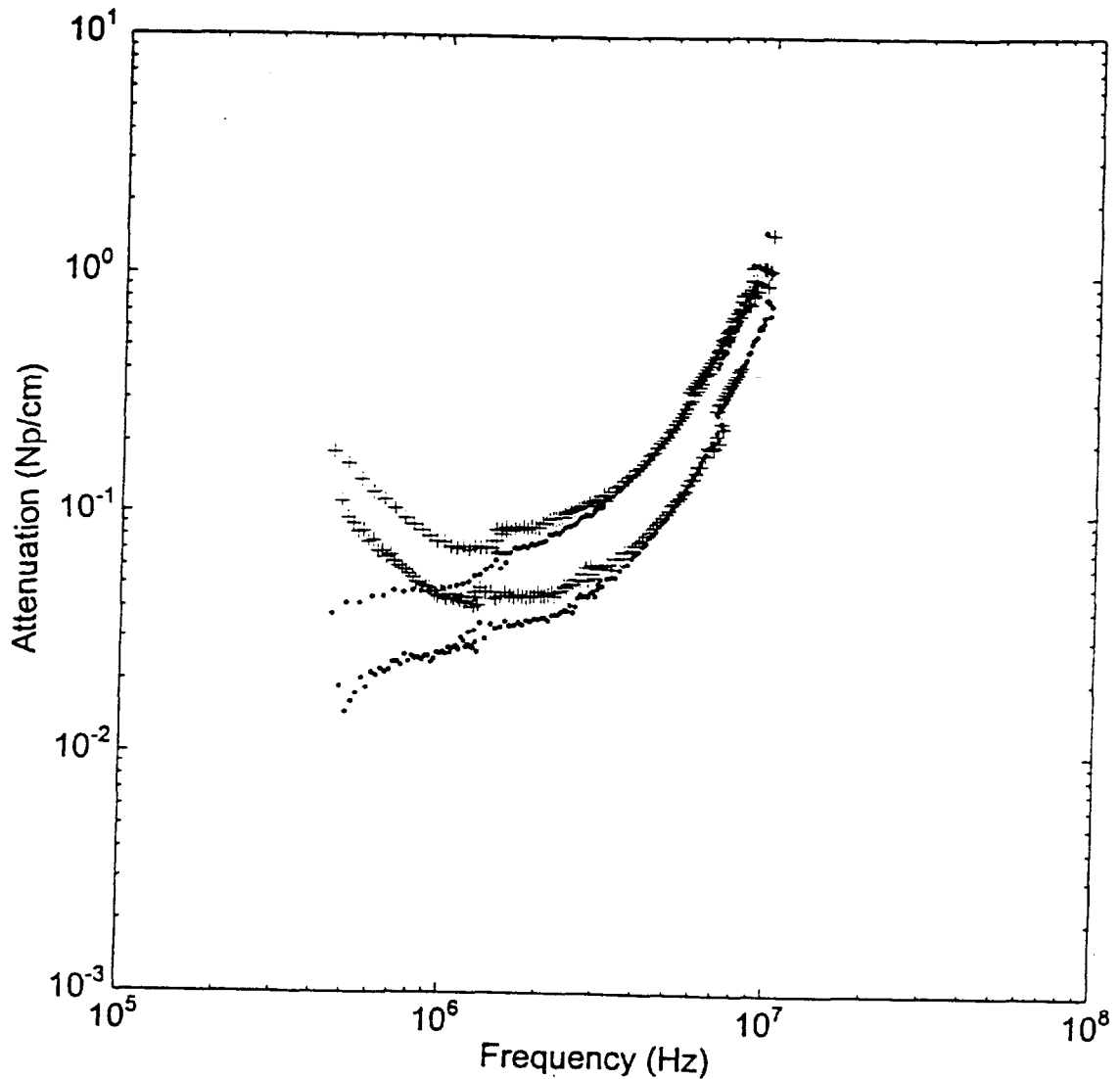


**Figure 7.2:** Attenuation versus frequency data for solid-gas-liquid systems of soda-lime glass beads in water at 5 % (lower curve) and 10 % solids by volume with bubbles generated by an electrolyzer at 40 V; 4 to 8 mA; <1 W. The solid-gas-liquid data (+) are shown with solid-liquid data (•) at the same solids concentrations. The solids size distribution has a mean radius of 14.9  $\mu\text{m}$  with standard deviation of 3.56  $\mu\text{m}$ . - E2231.

observed in Figure 7.1. There is enough vestigial evidence in the lower frequency (bubble attenuation dominated) region of the solid-gas-liquid attenuation spectra to suggest the presence of the bubble resonance peak at approximately 1 MHz. It should, again, be noted that the solid-gas-liquid attenuation curves in Figure 7.2 are not constant over a significant frequency range as seen in Figure 7.1. Rather, the attenuation curves go through a minimum at approximately 1.5 to 2 MHz, at which the attenuation due to the scattering by the solid particles begins to dominate the overall attenuation behavior of the slurry.

The most significant observation which can be made from Figures 7.1 and 7.2 is, as predicted by the theory for sound propagation in bubbly liquids, at sufficiently high frequencies, the attenuation due to the presence of the bubbles in solid-gas-liquid systems becomes so small as to be completely masked by that due to the solids. Therefore, by carefully choosing the frequency range of interrogation, it is possible to create conditions under which the presence of the gas bubbles (at small gas volume fraction) is essentially irrelevant, and the total attenuation is dominated by that of the solids. Also, in the event that some information about the size distribution and concentration of the bubbles is known *a priori*, it may be possible to predict the attenuation behavior of the bubbles and effectively subtract it from the overall measured attenuation caused by the solid-gas-liquid slurry. This approach would then yield the attenuation due to the solid-liquid slurry alone. This point will be addressed in more detail shortly.

Although it is not clear if the presence of the solids changes the gas phase volume fraction in the solid-gas-liquid slurry relative to the bubbly liquid alone, it appears that

the volume fraction of the solids does not affect the volume fraction of the bubbles in the system once the solids are present. This observation is made from examination of Figure 7.3. The figure shows experimental attenuation data for solid-gas-liquid systems with solids at 5 % and 10 % by volume. Also plotted are the attenuation curves predicted by the forward theory using the same solids volume fractions and size distribution as in the experiments and a log-normal bubble size distribution with a 23  $\mu\text{m}$  mean diameter and 4.3  $\mu\text{m}$  standard deviation. The bubble size distribution used in the forward theory predictions is determined by fitting the theory results to the experimental data. The bubble volume fraction in each forward theory prediction is held constant at  $1.5 \times 10^{-5}$ . It can be seen that both theoretical attenuation curves fit their respective experimental data reasonably well. The only difference between the conditions used in generating the two theory curves is in the volume fraction of the solids. When the solids volume fraction in the theory curves is adjusted for the increasing experimental volume fraction from 0.05 to 0.10, the fit between the theory prediction and experimental data is maintained. Therefore, although the volume fraction of the solids changes by a factor of two, the volume fraction of the gas bubbles remains unchanged. Thus the volume fraction of the solids does not appear to affect the bubble volume fraction in solid-gas-liquid slurries.

It has been previously mentioned that if some information about the bubble size distribution and volume fraction is known, it may be possible to predict the attenuation due to the bubbles in a solid-gas-liquid slurry and effectively subtract that attenuation from the total to yield just that due to the solids. This procedure has been carried out in Figure 7.4. This figure shows the result of subtracting the bubble attenuation from the

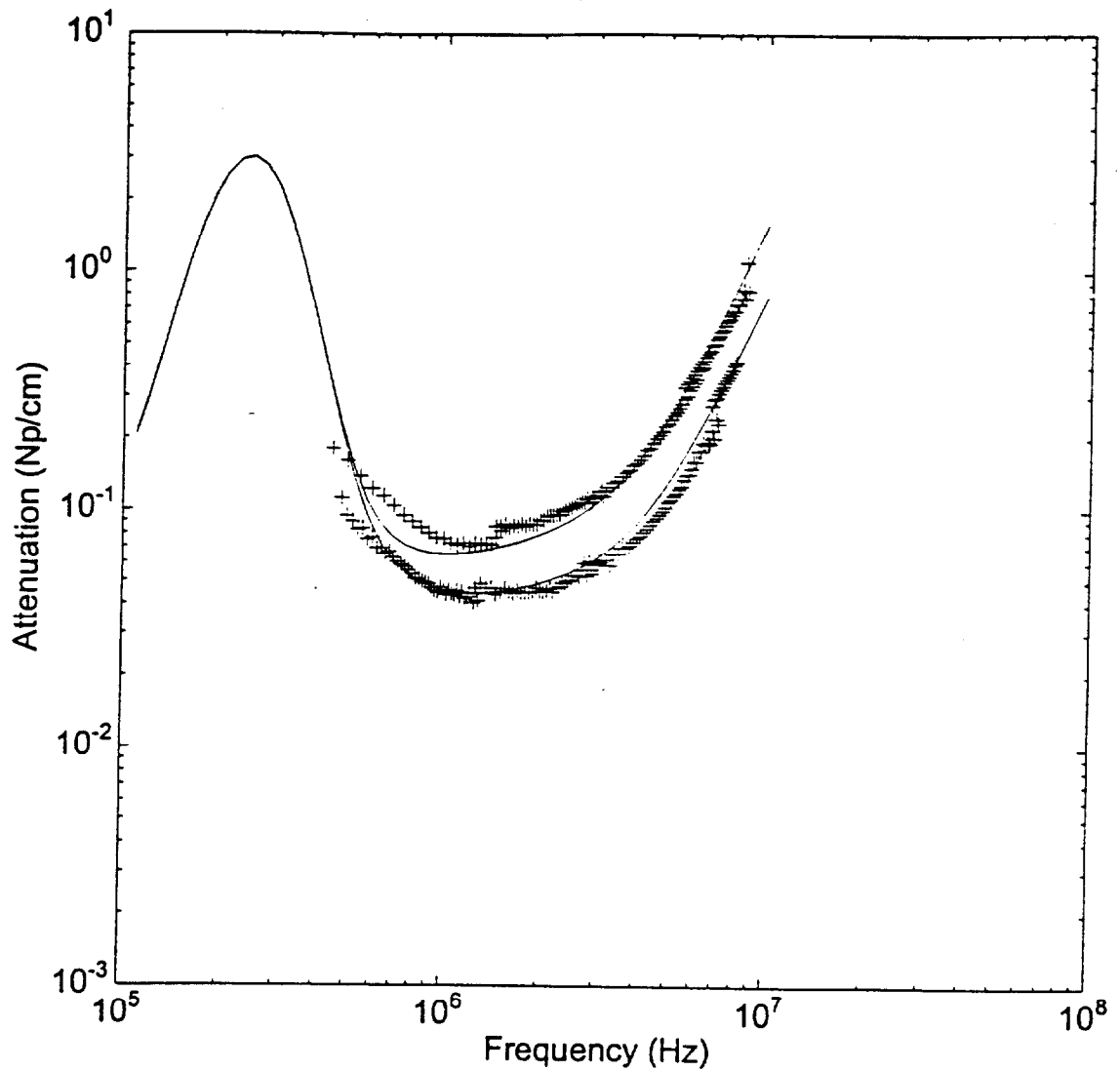


**Figure 7.3:** Comparison between experimental solid-gas-liquid attenuation data (+) at 5 % (lower curve) and 10 % solids (by volume) and forward problem theory predictions (solid curves) employing the same solids concentrations and a log-normal bubble size distribution with 23  $\mu\text{m}$  mean radius and 4.3  $\mu\text{m}$  standard deviation. The bubble volume fraction used in the theory predictions is  $1.5 \times 10^{-5}$ . - E2231.

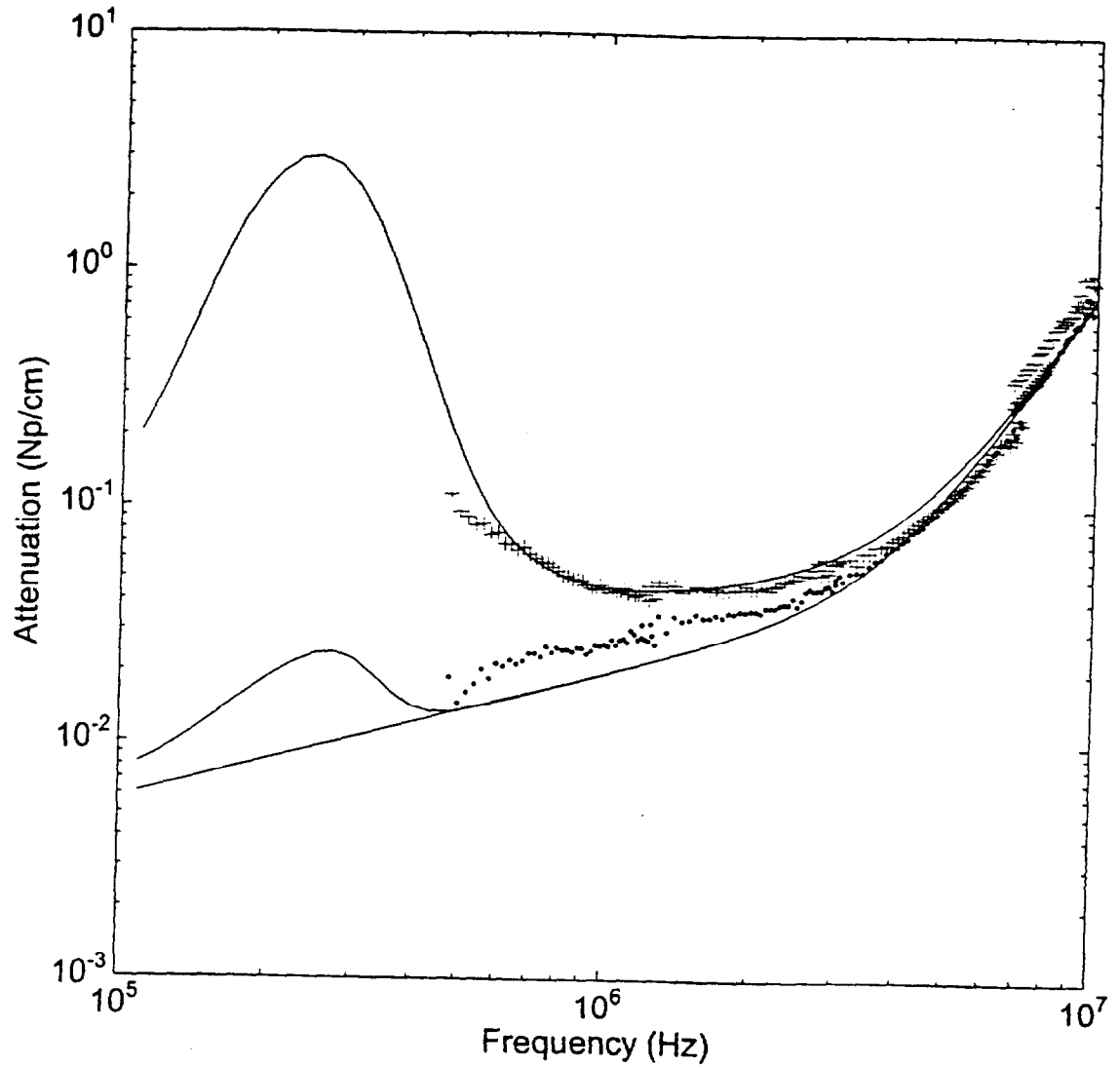


**Figure 7.4:** Results of predicting the attenuation due to the presence of bubbles in a solid-gas-liquid slurry and simply subtracting that attenuation from the total attenuation. The symbols represent experimental data for the solid-liquid ( $\bullet$ ) and solid-gas-liquid ( $+$ ) slurries, and the curves represent the forward theory predictions for those slurries and the difference after subtracting the bubble attenuation. - E2231.

total and compares it with the solid-liquid attenuation at 5 % solids by volume. The solid-gas-liquid forward theory attenuation curve is the same as that shown for the 5 % solids shown in Figure 7.3. It can be seen in this figure that the theory prediction resulting from the subtraction of the bubble attenuation from the total attenuation matches rather well with the solid-liquid data over the frequency range where those data are available. There is still a residual "hump" in the theory curve for the subtraction result at frequencies near the bubble resonance frequency. This "hump" is due to the non-linear volume fraction dependence of the bubble attenuation in this region which prevents simple subtraction from completely removing it from the total attenuation to yield only that due to the solids. However, the bubble resonance region is not the region of interest in this approach. It is the behavior in the "tail" region, well beyond the bubble resonance frequency which is of interest, and the subtraction of the bubble attenuation there yields results which compare fairly closely with the solid-liquid attenuation data.

As with the solid-liquid slurry experiments, it is of interest to investigate what effects, if any, would be contributed to the attenuation behavior of the slurry by a more elastic solid particle material, such as polystyrene. Therefore, further solid-gas-liquid attenuation experiments are attempted in systems containing polystyrene beads (Duke Scientific Corp., Palo Alto, CA) of 136  $\mu\text{m}$  mean diameter, with standard deviation of 13.5  $\mu\text{m}$ , in water. However, no data can be collected due to the presence of other physicochemical phenomena which interfere with the attenuation measurements. Attenuation measurements could be made in the solid-liquid only systems within the same experimental restrictions described previously. However, when bubbles are

introduced into the slurry via the limewood aerator, the polystyrene particles are carried by the gas bubbles to the surface of the liquid phase where a stable foam layer is formed. It is apparent that a dispersed air flotation system has been established. The process of dispersed air flotation is described by Burns *et al.* (1997). The foam layer is quite stable, and the polystyrene particles were intimately entrained within the surface foam layer. The foam layer does not allow bubbles entering the test cell from the bottom to escape, and bubbles from the surface foam layer are re-entrained when the slurry is mixed. The end result is a continuous increase in the gas phase volume fraction over the course of the attenuation measurement. This increase in the gas volume fraction soon causes the attenuation of the ultrasound in the slurry to become so large as to be unmeasurable.

Attempts have been made to rectify the flotation situation, such as washing the surfactant from the particles and varying the slurry pH to both the alkaline and acidic extremes. In all cases stable surface foam layers form when the gas is introduced, and there is visible flocculation of the polystyrene particles.

Some information can be gleaned from the polystyrene solid-gas-liquid experiments. The most prominent point is that, in the event that the density difference between the solid and liquid phase is small, gas entrained in the slurry will not be a major consideration in its characterization. The results of this set of experiments indicate that even at relatively small gas phase volume fraction, the gas bubbles will induce flotation of the solids and cause them to be removed from the slurry into a froth. The resulting problem of acoustic characterization of foams with entrained solids is beyond the scope of this work.

## Chapter 8: Conclusions and Future Work

### 8.1 Conclusions:

The theory of Allegra and Hawley (1972) for dilute suspensions is shown to be in excellent agreement with experimental attenuation data obtained for slurries of soda-lime glass spheres in water and polystyrene spheres in water.

An effective medium approximation for the attenuation in concentrated slurries is employed in which the equations of motion are derived in a manner similar to that used in the dilute theory. However, the effective medium approach considers a solid particle to be centered inside a pure liquid "shell". Results of the effective medium approximation are compared with data obtained in fairly concentrated slurries, of up to 50 % solids by volume, of 125  $\mu\text{m}$  mean diameter Potter's Beads (soda-lime glass) in a mixture of glycerin and water. The agreement between the effective medium approximation and the experimentally obtained attenuation data is quite good up to volume fractions of approximately 0.30. At higher volume fractions, there is significant deviation.

In solid-gas-liquid slurries it is determined that, at sufficiently high frequencies, the total attenuation of ultrasound in the slurry is dominated by the attenuation due to the solid particles. In addition, the bubble volume fraction in the solid-gas-liquid system is not affected by the volume fraction of the solid particles. It is also determined that, if the bubble size distribution and volume fraction are known *a priori*, the attenuation due to the bubbles in a solid-gas-liquid slurry may be simply subtracted from the total

attenuation in the slurry to yield only that due to the solids at frequencies well beyond the bubble resonance frequency.

Tikhonov regularization and linear programming techniques are employed to solve the inverse problem of determining the particle volume fraction distribution from the attenuation versus frequency data. Although these techniques are successful in solving the inverse problem in several cases, it is also shown that the results are very sensitive to the choice of frequency range, the physical properties of the particles, and the nature of the particle volume fraction distribution (unimodal, bimodal, etc.). Since the same techniques were shown to work quite well for bubbly liquids, the failures in the technique results which did occur are attributed to the complex resonance behavior of the slurries.

## **8.2 Recommendations for Future Work:**

The work which is recommended to further the progress of this area of study can be divided into three categories. The first category consists of work which will advance the development of the acoustic probe within the current scope of its development. The second category is work which is recommended to broaden the scope of the acoustic probe development project. The final category is work which is recommended to enhance the performance of the photomicrographic imaging system.

The current status of efforts to solve the inverse problem for solid-liquid slurries indicates that the inverse problem for these systems is far more difficult to solve than for other systems, such as bubbly liquids. This difficulty arises due to the complicated and

multiple resonances exhibited by the solid particles. It is found that satisfactory inverse problem results can only be obtained for solid-liquid systems where the solid phase is of a somewhat elastic material, such as polystyrene. The lack of distinct separation between the various modes of resonance in glass particles makes satisfactory solution of the inverse problem impossible in those systems. Therefore, it is most desirable to obtain solid-liquid-gas attenuation data for systems where the solid phase consists of a more elastic material, such as polystyrene particles. The success in solution of the inverse problem for solid-liquid systems of this nature indicates that similar systems should be ideal for investigating the possibility of solving the inverse problem for solid-gas-liquid systems of similar composition. It is recommended that solid-gas-liquid attenuation experiments be attempted in systems containing particles of another material, such as polymethylmethacrylate (PMMA) or another system where flotation problems will be avoided. With a density of  $1.19 \text{ g/cm}^3$  (as opposed to  $1.05 \text{ g/cm}^3$  for polystyrene), the PMMA particles are less likely to be carried to the surface by the gas bubbles; yet the density is still close enough to that of water to facilitate homogeneous suspension. Also, the PMMA is a polymeric material which should be more elastic than glass. Therefore, there should be the desired separation between the resonances of the individual modes of oscillation which made the solution of the inverse problem for polystyrene/water solid-liquid systems possible.

A fluidized bed or other flow system apparatus allows for better control of the slurry properties. A system of this type is preferable if more economical solid particles could be acquired to facilitate such an apparatus.

Another area where further investigation is recommended is in the use of lower frequency transducers. Now that initial investigation has shown that the currently used methods of bubble generation create bubbles with resonance frequencies in the range of 0.03 to 0.5 MHz, it would be advisable to employ transducers which operate in these frequency ranges. Acquisition of solid-gas-liquid data down to these frequency ranges would provide information about the bubble resonance peaks which would better delineate the contributions of the gas bubbles to the solid-gas-liquid attenuation behavior. Also, implementation of these lower frequency transducers may also provide a means for collecting more reliable bubbly liquid attenuation data.

In regard to expansion of the scope of the acoustic probe development program, it is recommended that solid-liquid experimentation be revisited for the purpose of examining the acoustic behavior of very dilute (less than 1 % solids by volume) solid-liquid suspensions.

Another possible direction in which the probe development may proceed in the future could be an investigation of the propagation of acoustic energy in foams. These foams could be both gas-liquid only and, as has been observed in this study, gas-liquid with entrained solids. Another method to characterize such systems could be useful.

The final area where a considerable amount of future work can be done is in regard to the photomicrographic video imaging system. The current status of the imaging system allows for making multiple frame "movies" of bubbles and particles. Measurement of bubble sizes can be performed and recorded manually with reasonable accuracy. However, the combined hardware and software capabilities of this system offer

the potential for far more accurate and efficient bubble and particle size measurements through automation.

The *Image SXM* software package allows for many manipulations of an acquired image and has the capability to provide an automated measurement of bubble or particle size distributions. However, completion of these tasks will require the creation of user-written “macros”, or short program codes which instruct the computer software to perform operations which would normally be performed manually at the keyboard. A user will need to create “macros” to perform the necessary thresholding, conversion to binary image, bubble/particle distribution measurement, and presentation of data, and/or writing of data to data files for computer storage.

Another issue in regard to the imaging system is determining the proper lighting which should be used under experimental conditions to obtain the clearest photographs of the bubbles or particles with the best resolution of the bubble/particle interface with the liquid, or what is referred to as a large edge gradient (Bongiovanni *et al.* 1997). Indeed, there may not be a single lighting arrangement which will allow for optimum photo resolution of both the bubbles and particles in a solid-gas-liquid system. It is recommended that a study be performed to examine, in detail, the advantages and disadvantages of different lighting configurations as described in the literature in order to construct an overall imaging system which will provide for optimum use of the existing equipment.

## References

- Alba, E., "Method and Apparatus for Determining Particle Size Distribution and Concentration in a Suspension Using Ultrasonics," *US Patent No. 5,121,629* (1992).
- Allegra, J. R. and Hawley, S. A., "Attenuation of Sound in Suspensions and Emulsions: Theory and Experiments," *J. Acoust. Soc. Am.* **51**, 1545 (1972).
- Atkinson, C. M., "Acoustic Wave Propagation and Non-Intrusive Velocity Measurements in Highly Concentrated Suspensions," D.Sc. Thesis, Mass. Inst. Technol., Cambridge (1991).
- Atkinson, C. M., and Kytomaa, H. K., "Acoustic Wavespeed and Attenuation in Suspensions," *Int. J. Multiphase Flow.* **18**, 577 (1993).
- Bapat, P. M., "Mass Transfer in a Liquid-Liquid Continuous-Flow Stirred-Tank Reactor," Ph.D. Thesis, Ill. Inst. Technol., Chicago (1982).
- Barrett, S., *Image SXM v1.61-7 Image Analysis Software*, University of Liverpool, England (1998).
- Bolz, R. E., *CRC Handbook of Tables for Applied Engineering Science* (CRC Press, Boca Raton, FL, USA, 1973).
- Bongiovanni, C., Chevaillier, J. Ph., and Fabre, J., "Sizing of Bubbles by Incoherent Imaging: Defocus Bias," *Experiments in Fluids* **23**, 209 (1997).
- Bonnet, J. C. and Tavlarides, L., L., "Ultrasonic Technique for Dispersed Phase Hold-Up Measurements," *I & EC Res.* **26**, 811 (1987).
- Burns, S. E., Yiacomou, S., and Tsouris, C., "Microbubble Generation for Environmental and Industrial Separations," *Separation and Purification Technology* **11**, 221 (1997).
- Carstensen, E. L. and Foldy, L. L., "Propagation of Sound Through a Liquid Containing Bubbles," *J. Acoust. Soc. Am.* **19**, 481 (1947).
- Chivers, R. C. and Anson, L. W., "Calculations of the Backscattering and Radiation Force Functions of Spherical Targets for Use in Ultrasonic Beam Assessment," *Ultrasonics* **20**, 25 (1982).

- Commander, K. W. and McDonald, R. J., "Finite-element Analysis Solution of the Inverse Problem in Bubble Swarm Acoustics," *J. Acoust. Soc. Am.* **89**, 592 (1991).
- Commander, K. W. and Prosperetti, A., "Linear Pressure Waves in Bubbly Liquids: Comparison Between Theory and Experiment," *J. Acoust. Soc. Am.* **85**, 732 (1989).
- Delves, L. M. and Mohamed, J. L., *Computational Methods for Integral Equations* (Cambridge University Press, Cambridge, England, 1985).
- Dodd, T. L., Hammer, D. A., Sangani, A. S. and Koch, D. L., "Numerical Simulations of the Effect of Hydrodynamic Interactions on Diffusivities of Integral Membrane Proteins", *J. Fluid Mech.*, **293**, 147 (1995).
- Duraiswami, R., "Bubble Density Measurement Using an Inverse Acoustic Scattering Technique," ASME Cavitation and Multiphase Forum, Washington, DC, edited by O. Furuya, FED vol. 153, p. 67, (ASME, New York, 1993).
- Duraiswami, R., Prabhukumar, S. and Chahine, G. L., "Bubble Counting Using an Inverse Acoustic Scattering Method," *J. Acoust. Soc. Am.*, **104**, 2699 (1998).
- Epstein, P. S. and Carhart, R. R., "The Absorption of Sound in Suspensions and Emulsions. I. Water Fog in Air," *J. Acoust. Soc. Am.* **25**, 553 (1953).
- Faran, J. J., "Sound Scattering by Solid Cylinders and Spheres," *J. Acoust. Soc. Am.* **23**, 405 (1951).
- Foldy, L. L., "The Multiple Scattering of Waves," *Phys. Rev.* **67**, 107 (1945).
- Garr, D., "Too Hot to Handle," *Popular Science* **52**, August 1992.
- Gradshteyn, I. S., and Ryzhik, I. M., *Tables of Integrals, Series, and Products*, 5<sup>th</sup> Edition, Academic Press (1994).
- Greenwood, M. S., Mai, J. L., and Good, M. S., "Attenuation Measurements of Ultrasound in a Kaolin-Water Slurry: A Linear Dependence Upon Frequency," *J. Acoust. Soc. Am.* **94**, 908 (1993).
- Happel, J. and Brenner, H., *Low Reynolds Number Hydrodynamics*, Martinus Nijhoff Publishers, Dordrecht, The Netherlands, (1973).

- Jeffrey, D. J., "Conduction Through a Random Suspension of Spheres", *Proc. R. Soc. Lond. A*, **335**, 355 (1973).
- Kessler, L. W., Hawley, S. A., and Dunn, F., "Semiautomatic Determination of Ultrasonic Velocity and Absorption," *Acoustica* **24**, 105 (1971).
- Kim, S., and Russel, W. B., "Modeling of Porous Media by Renormalization of the Stress Equations", *J. Fluid Mech.*, **154**, 269 (1995).
- Kinsler, L. E., Frey, A. R., Coppens, A. B., and Sanders, J. V., *Fundamentals of Acoustics* (John Wiley & Sons, Inc., New York, NY, USA, 1982).
- Kirou, V. I., Tavlarides, L. L., Bonnet, J. C., and Tsouris, C., "Flooding, Holdup, and Drop Size Measurement in a Multistage Column Extractor," *AIChE Journal* **34**, 283 (1988).
- Kol'tsova, I. S., Krynskii, L. O., Mikhalov, I. G. and Pokrovskaya, I. E., "Attenuation of Ultrasonic Waves in Low-Viscosity Liquids Containing Gas Bubbles," *Akust. Zh.* **25**, 725 (1979) [English Translation: *Sov. Phys. Acoust.* **25**, 409 (1979)].
- Kress, R., *Linear Integral Equations* (Springer, Berlin, Germany, 1989).
- Kuster, G., and Toksoz, M. N., "Velocity and Attenuation of Seismic Waves Waves in Two-Phase Media: Part II. Experimental Results," *Geophysics*, **39**, 607 (1974).
- Kuwabara, S., "The Forces Experienced by Randomly Distributed Parallel Circular Cylinders or Spheres in a Viscous Flow at Small Reynolds Numbers", *J. Phys. Soc. Japan*, **14**, 527 (1959).
- Kytomaa, H. K., "Theory of Sound Propagation in Suspensions: A Guide to Particle Size and Concentration Characterization," *Powder Technol.* **82**, 115 (1995).
- Ladd, A. J. C., "Hydrodynamic Transport Coefficients of Random Dispersions of Hard Spheres", *J. Chem. Phys.*, **93**, 3484 (1990).
- Landau, L. D. and Lifshitz, E. M., *Theory of Elasticity*, 3<sup>rd</sup> Edition, Pergamon Press (1986).
- Levi, B. G., "Hanford Seeks Short- and Long-term Solutions to Its Legacy of Waste," *Physics Today*, 17 March 1992.

- Lighthill, M. J., "Viscosity Effects in Sound Waves of Finite Amplitude," in *Surveys in Mechanics*, edited by G. K. Batchelor and R. M. Davies (Cambridge University Press, Cambridge, England, 1956).
- Ma, Y., Varadan, V. K. and Varadan, V. V., "Comments on Ultrasonic Propagation in Suspensions," *J. Acoust. Soc. Am.* **87**, 2779 (1990).
- Martin, J., Rakotomalala, N., and Salin, D., "Hydrodynamic Dispersion of Noncolloidal Suspensions: Measurement form Einstein's Argument," *Phys. Rev. Lett.* **74**, 1347 (1995).
- McClements, D. J., "Comparison of Multiple Scattering Theories with Experimental Measurements in Emulsions," *J. Acoust. Soc. Am.* **91**, 849 (1992).
- McLeod, F., "Directional Doppler Flowmeter," *Intl. Conf. Med. Bio. Eng.* Stockholm, Sweden 213 (1967).
- Mo, G., and Sangani, A. S., "A Method for Computing Stokes Flow Interactions Among Spherical Objects and Its Application to Suspensions of Drops and Porous Particles", *Phys. Fluids*, **6**, 1637 (1994).
- Oja, T. and Alba E., "Acoustic Attenuation Spectroscopy for Particle Sizing of High Concentration Dispersions," presentation at the *NIST International Workshop on Ultrasonic and Dielectric Characterization Techniques for Suspended Particulates*. (Gaithersburg, MD, USA, 1997).
- Okamura, S., Uchida, S., Katsumata, T., and Iida, K., "Measurement of Solids Holdup in a Three-Phase Fluidized Bed by an Ultrasonic Technique," *Chem. Eng. Sci.* **44**, 196 (1989).
- Pacek, A. W., Moore, I. P. T., Nienow, A. W., and Calabrese, R. V., "Video Technique for Measuring Dynamics of Liquid-Liquid Dispersion During Phase Inversion," *AIChE Journal* **40**, 1940 (1994).
- Perry, R. H., Green, D. W., and Maloney, J. O., (Eds.), *Perry's Chemical Engineer's Handbook*, (McGraw-Hill, New York, NY, USA; 1984).
- Ramirez, R. W., *The FFT - Fundamentals and Concepts* (Prentice Hall, Englewood Cliffs, NJ, USA, 1985).
- Sangani, A. S., "A Pairwise Interaction Theory for Determining the Linear Acoustic Properties of Dilute Bubbly Liquids," *J. Fluid Mech.* **232**,

221 (1991).

- Sangani, A. S., Zhang, D. Z., and Prosperetti, A., "The Added Mass, Basset, and Viscous Drag Coefficients in Nondilute Bubbly Liquids Undergoing Small-Amplitude Oscillatory Motion," *Phys. Fluids A* **3**, 2955 (1991).
- Sangani, A. S. and Mo, G., "Elastic Interactions in Particulate Composites with Perfect as Well as Imperfect Interfaces", *J. Mech. Phys. Solids* **45**, 2001 (1997).
- Shin, W-T, Yiacoumi, S., and Tsouris, C. "Experiments on Electrostatic Dispersion of Air in Water," *I & EC Res.* **36**, 3647 (1997).
- Silberman, E., "Sound Velocity and Attenuation in Bubbly Mixtures Measured in Standing Wave Tubes," *J. Acoust. Soc. Am.* **29**, 925 (1957).
- Soong, Y., Blackwell, A. G., Schehl, R. R., Zarochak, M. F., and Rayne, J. A., "Ultrasonic Characterization of Three-Phase Slurries", *Chem. Eng. Comm.*, **138**, 213 (1995).
- Soong, Y., Gamwo, I. K., Blackwell, A. G., Harke, F. W., Schehl, R. R., and Zarochak, M. F., "Ultrasonic Characterization of Slurries in an Autoclave Reactor at Elevated Temperature", *I & EC Res.*, **35**, 1807 (1996).
- Spelt, P. D. M., Norato, M. A., Sangani, A. S., and Tavlarides, L. L., "Determination of Particle Size Distributions from Acoustic Wave Propagation Measurements", accepted for publication in *Phys. Fluids*, January (1999).
- Spelt, P. D. M., Norato, M. A., Sangani, A. S., Tavlarides, L. L., and Greenwood, M. S., "Attenuation of Sound Waves in Concentrated Slurries: An Effective-Medium Theory and Experiments", in preparation (1999).
- Strout, T. A., "Attenuation of Sound in High-Concentration Suspensions: Development and Application of an Oscillatory Cell Model," Ph.D. Thesis, University of Maine, Orono (1991).
- Tavlarides, L. L., and Bonnet, J. C., "An Ultrasonic Technique for Dispersed Phase Holdup Measurements," *US Patent No. 4,726,221* (1988).
- Tsouris, C., and Tavlarides, L. L., "Comments on 'Model for Hold-Up Measurements in Liquid Dispersions Using an Ultrasonic Technique'," *I & EC Res.* **29**, 2170 (1990).
- Tsouris, C., and Tavlarides, L. L., "Volume Fraction Measurements of Water in Oil by an Ultrasonic Technique," *I & EC Res.* **32**, 998 (1993).

- Tsouris, C., Norato, M. A., and Tavlarides, L. L., "A Pulse-Echo Ultrasonic Probe for Local Volume Fraction Measurements in Liquid-Liquid Dispersions," *I & EC Res.* **34**, 3154 (1995).
- Tsouris, C., DePaoli, D. W., Feng, J. Q., and Scott, T. C., "Experimental Investigation of Electrostatic Dispersion of Nonconductive Fluids into Conductive Fluids," *I & EC Res.* **34**, 1394 (1995).
- Turner, J. C. R., "Two-Phase Conductivity, the Electrical Conductance of Liquid Fluidized Beds of Spheres", *Chem. Eng. Sci.* **31**, 487 (1976).
- Uchida, S., Okamura, S., and Katsumata, T., "Measurement of Longitudinal Distribution of Solids Holdup in a Three-Phase Fluidized Bed by Ultrasonic Technique," *Can. J. Chem. Eng.* **67**, 166 (1989).
- Urick, R. J., "Sound Velocity Method for Determining the Compressibility of Finely Divided Substances," *J. Appl. Physics* **18**, 983 (1947).
- Urick, R. J., "The Absorption of Sound in Suspensions of Irregular Particles," *J. Acoust. Soc. Am.* **20**, 283 (1948).
- Varadan, V. K., Bringi, V. N., Varadan, V. V., and Ma, Y., "Coherent Attenuation of Acoustic Waves by Pair-Correlated Random Distribution of Scatterers with Uniform and Gaussian Size Distributions," *J. Acoust. Soc. Am.* **73**, 1941 (1983).
- Wang, W. and Sangani, A. S., "Nusselt Number for Flow Perpendicular to Arrays of Cylinders in the Limit of Small Reynolds and Large Peclet Numbers", *Phys. Fluids*, **9**, 1529 (1997).
- Weast, R. C., Astle, M. J., and Beyer, W. H., (Eds.), *CRC Handbook of Chemistry and Physics*, (CRC Press, Boca Raton, FL, USA 1984).
- Yi, J. H., and Tavlarides, L. L., "Model for Hold-Up Measurements in Liquid-Liquid Dispersions Using an Ultrasonic Technique," *I & EC Res.* **29**, 475 (1990).

## **Appendix A: Boundary Conditions from Epstein and Carhart (1953) and Allegra and Hawley(1972)**

Given in this Appendix is a set of linear equations for unknowns which include the coefficients,  $A_n$ , required to calculate the attenuations from equations (2.59) and (2.66) through (2.68), or (2.69). These equations are derived from the boundary conditions on the surface of a test particle. In addition to the coefficients,  $A_n$ , and  $\tilde{A}_n$ , of the solution of equation (2.46) outside and inside the particle, respectively; similar coefficients arise due to the solutions of equations (2.47) and (2.48), denoted by  $B_n$  and  $C_n$ , respectively. It should be noted that equation (2.48) is an equation for the vector  $\mathbf{A}$ , rather than for a scalar velocity potential, but only the azimuthal component of  $\mathbf{A}$  is non-zero. Therefore, the solution of equation (2.48) has only the scalar coefficient,  $C_n$ . The following notations are relevant to the equations presented here:  $z_c = k_c a$ ,  $z_T = k_T a$ ,  $z_s = k_s a$ .

$$z_c j'_n(z_c) + A_n z_c h'_n(z_c) + B_n z_T h'_n(z_T) - C_n n(n+1) h_n(z_s) = \tilde{A}_n \tilde{z}_c j'_n(\tilde{z}_c) + \tilde{B}_n \tilde{z}_T j'_n(\tilde{z}_T) - \tilde{C}_n n(n+1) j_n(\tilde{z}_s) \quad (\text{A.1})$$

$$j_n(z_c) + A_n h_n(z_c) + B_n h_n(z_T) - C_n (h_n(z_s) + z_s h'_n(z_s)) = \tilde{A}_n j_n(\tilde{z}_c) + \tilde{B}_n j_n(\tilde{z}_T) - \tilde{C}_n (j_n(\tilde{z}_s) + \tilde{z}_s j'_n(\tilde{z}_s)) \quad (\text{A.2})$$

$$b_c [j_n(z_c) + A_n h_n(z_c)] + B_n b_T h_n(z_T) = \tilde{A}_n \tilde{b}_c j_n(\tilde{z}_c) + \tilde{B}_n \tilde{b}_T j_n(\tilde{z}_T) \quad (\text{A.3})$$

$$\tau (z_c b_c [j'_n(z_c) + A_n h'_n(z_c)] + B_n b_T z_T h'_n(z_T)) = \tilde{\tau} (\tilde{A}_n \tilde{b}_c \tilde{z}_c j'_n(\tilde{z}_c) + \tilde{B}_n \tilde{b}_T \tilde{z}_T j'_n(\tilde{z}_T)) \quad (\text{A.4})$$

$$\begin{aligned} & (-i\omega\mu) \left( \left[ (z_s^2 - 2z_c^2) j_n(z_c) - 2z_c^2 j''_n(z_c) \right] + \right. \\ & A_n \left[ (z_s^2 - 2z_c^2) h_n(z_c) - 2z_c^2 h''_n(z_c) \right] + \\ & B_n \left[ (z_s^2 - 2z_T^2) h_n(z_T) - 2z_T^2 h''_n(z_T) \right] + \\ & C_n 2n(n+1) [z_s h'_n(z_s) - h_n(z_s)] \Big) = \\ & \tilde{A}_n \left[ (\omega^2 \tilde{\rho} a^2 - 2\tilde{\mu} \tilde{z}_c^2) j_n(\tilde{z}_c) - 2\tilde{\mu} \tilde{z}_c^2 j''_n(\tilde{z}_c) \right] + \\ & \tilde{B}_n \left[ (\omega^2 \tilde{\rho} a^2 - 2\tilde{\mu} \tilde{z}_T^2) j_n(\tilde{z}_T) - 2\tilde{\mu} \tilde{z}_T^2 j''_n(\tilde{z}_T) \right] + \\ & \tilde{C}_n 2\tilde{\mu} n(n+1) [\tilde{z}_s j'_n(\tilde{z}_s) - j_n(\tilde{z}_s)] \end{aligned} \quad (\text{A.5})$$

$$\begin{aligned}
& (-i\omega\mu)(z_c j'_n(z_c) - j_n(z_c) + A_n[z_c h'_n(z_c) - h_n(z_c)] + \\
& B_n[z_T h'_n(z_T) - h_n(z_T)] - \\
& (C_n/2)[z_s^2 h''_n(z_s) + (n^2 + n - 2)h_n(z_s)]) = \quad (A.6) \\
& \tilde{\mu}(\tilde{A}_n[\tilde{z}_c j'_n(\tilde{z}_c) - j_n(\tilde{z}_c)] + \tilde{B}_n[\tilde{z}_T j'_n(\tilde{z}_T) - j_n(\tilde{z}_T)] - \\
& (\tilde{C}_n/2)[\tilde{z}_s^2 j''_n(\tilde{z}_s) + (n^2 + n - 2)j_n(\tilde{z}_s)]).
\end{aligned}$$

Here,  $b_c$  and  $b_T$  are given by

$$b_c = \frac{(1-\gamma)\omega^2}{\beta c^2}, \quad b_T = -\frac{\gamma}{c_1^2 \beta} \left[ \omega^2 - \left( \frac{c_1^2}{\gamma} - \frac{4i\omega\mu}{3\rho} \right) k_T^2 \right], \quad (A.7)$$

where  $\beta$  is the thermal expansion coefficient and  $c_1$  is the liquid equivalent speed of sound for spherical compressional waves in an elastic isotropic solid given by

$$\tilde{c}_1 = \sqrt{(\tilde{\lambda} + 2\tilde{\mu}/3)/\tilde{\rho}}. \quad \text{The Lamé constant, } \tilde{\lambda}, \text{ is not really needed when the speed of}$$

sound,  $c$ , of the longitudinal compressional waves is specified, as one can also write

$$\tilde{c}_1^2 = c^2 \left( 1 - 4\tilde{\mu}/(3\rho c^2) \right). \quad \text{The above equations have also been given by Epstein and}$$

Carhart (1953) and Allegra and Hawley (1972). However, in both there are typographical

errors. In Epstein and Carhart (1953), the last  $j'_n(\tilde{z}_s)$  in equation (A.2) is erroneously

replaced by  $h'_n(\tilde{z}_s)$ . In Allegra and Hawley (1972), the signs of both

$(n^2 + n - 1)$  terms are wrong, and the  $h_n(z_s)$  term on the left-hand side of equation

(A.6) has an argument  $\tilde{z}$  instead. Also, the first  $z_s$  after  $C_n$  is replaced by  $\tilde{z}_s$ . Not

correcting the typographical errors in Allegra and Hawley (1972) would alter the results significantly.

## **Appendix B: Experimental Procedures**

### **B.1 Slurry Attenuation Measurement Procedure:**

#### **B.1.1 General Considerations:**

In all attenuation measurement experiments, regardless of which type of vessel or cell is being used, it is imperative that the separation distance between each transducer pair be measured once the transducers are installed. The vessel or test cell should be clean and dry. The electronics and instrumentation should be set up as per Figures 3.2 and 3.4, depending upon whether the Toneburst or FFT/Pulse Technique is being employed. It is recommended that, whenever possible, data should be acquired by both techniques as agreement between results of the two techniques provides reproducibility of results. Also, the Toneburst Technique provides slightly better results at higher frequencies and larger attenuations where significant noise in the data may interfere with FFT calculations. Conversely, the FFT/Pulse Technique seems to provide slightly better results at lower frequencies and lower attenuations where the error the difference between the slurry and reference water voltage signals is so small that the error in the measurement is of the same order of magnitude as the measurement, itself. This is the trend that was seen in earlier attenuation experiments; however, later toneburst measurements were performed by having the oscilloscope make the peak-to-peak voltage measurement on a waveform averaged over 50 sweeps, rather than making manual peak-to-peak voltage measurements in real time. Allowing the oscilloscope to make the

measurements does improve the data quality for the Toneburst Technique at lower frequencies and attenuations.

It should also be noted that earlier attenuation measurements refer to a "Standard" Toneburst Technique. This technique is just the toneburst technique described in Section 3.1.2, with the received signal going through an attenuator box, to the receiver/amplifier of the TB-1000 card, then on to the oscilloscope. This variation of the Toneburst Technique has been all but abandoned as it is sometimes difficult to achieve consistent receiver/amplifier performance. Secondly, in most cases it was found that the use of the receiver/amplifier was unnecessary, and better (more accurate and reproducible) results are achieved when the received signal is input directly to the oscilloscope. This variation of the Toneburst Technique is the "Direct" Toneburst Technique. The "Direct" method is the preferred Toneburst procedure, and it is the method which has been (and should be) employed, unless noted otherwise.

In regard to the operation of the electronic instrumentation, it is not the objective of this work to reproduce information which is available in the various user's manuals. The objective is, rather, to document information which is conducive to obtaining quality experimental results, yet is NOT available or clear in the user's manuals. The contents of this work should not be construed as to obviate the use of user's manuals.

### **B.1.2 Operation of the Matec TB-1000 Toneburst Generator and**

#### **Panametrics 5052 PR Pulser/Receiver:**

### **B.1.2.1 Matec TB-1000 Toneburst Generator:**

The Matec TB-1000 toneburst generator is a digital synthesizer card installed in the Gateway 2000 P5-66 data acquisition computer. It is used as the signal generator for all measurements pertaining to the Toneburst Technique. The operation of the TB-1000 is fairly straightforward as the software is entirely menu driven. However, there is also a user's manual available in the laboratory.

The TB-1000 is accessed by closing Windows and obtaining a DOS prompt. Change the directory to the TB-1000 directory by typing `CD\TB1000` at the `C:\>` prompt. Once in the TB-1000 directory, the driver software may be started by typing `MATEC` at the `C:\TB1000>` prompt. The software will now start running and the toneburst card can be turned on by choosing the TB-1000 menu choice. As the "Direct" toneburst method will usually be the method used, the user need only adjust the frequency of the output signal and the pulse width to suit experimental conditions. More detailed operation instructions are provided in the user's manual if necessary.

The overall experimental set up is shown schematically in Figure 3.2. Measurements should be made at frequencies spaced fairly evenly over the operational range of each transducer pair. It is usually preferable to turn on the toneburst card approximately one half hour prior to making measurements so that the card has time to "warm up". Also, it is advisable to always have some transducer connected to the "PULSE OUT" connector on the back of the computer so that the toneburst card is always "seeing" some load while the power is on. If the measurement transducers are

disconnected and the toneburst generator is on, an old transducer can be connected in place of the measurement transducers. IT IS ALSO IMPORTANT TO TURN OFF THE VOLTAGE TO THE TONEBURST CARD (via the software menu) BEFORE CONNECTING OR DISCONNECTING ANY CABLES. The TB-1000 outputs several hundred volts.

### **B.1.2.2 Panametrics 5052PR Pulser/Receiver:**

All signals used in the FFT/Pulse technique are generated by the Panametrics 50502PR Pulser/Receiver. It is a relatively simple instrument to operate, and it also has a user's manual available in the laboratory. The pulser/receiver is always operated in the "pitch-catch" mode. This implies that the transmitter transducer will be connected at the T/R connector, and the receiver transducer will be connected at the RCVR connector. The general experimental set up is shown schematically in Figure 3.4 The pulser control settings (as they appear on the Pulser/Receiver unit) which have been determined to yield the best results for attenuation measurements are as follows:

REP. RATE = 0 (Lowest setting possible WITHOUT being on MIN/EXT)

ENERGY = 4

ATTEN (dB) = Variable: Setting which is appropriate for experimental conditions.

H.P. FILTER = OUT

DAMPING = Variable: Setting depends upon transducer pair used.

The 1 MHz transducers operate best at a setting of about

4. The 2.25 MHz, 5 MHz, 7.5 MHz, and 10 MHz transducers operate best at a setting of 10.

GAIN (dB) = 40

### **B.1.3 Operation of the LeCroy 9310A Dual 400 MHz (Digital)**

#### **Oscilloscope:**

All acoustic signals obtained in this study are acquired by a LeCroy 9310A digital oscilloscope. When compared to earlier models of digital oscilloscopes from various manufacturers, the LeCroy 9310A is rather simple and intuitive to operate. All of the functions of which the oscilloscope are capable are menu driven, and a clear and concise user's manual is available in the laboratory. It is recommended that anyone who is not familiar with this particular model of oscilloscope take the time to perform the tutorial provided by the manufacturer in the user's manual. This tutorial demonstrates all of the major capabilities of the oscilloscope.

An important detail about proper operation of the oscilloscope is that all input channels (Channels 1 and 2) should be set for a coupling impedance of 50  $\Omega$  DC. It is also important to make sure that the oscilloscope is being triggered properly by either the toneburst card (coaxial cable connecting "TRIGGER" connector on toneburst card and "EXT" connector on the front of the oscilloscope) or the pulser/receiver (coaxial cable connecting "+SYNC" connector on pulser/receiver and "EXT" connector on the

oscilloscope). The trigger should be set at positive slope, external trigger, DC coupling at 1 M $\Omega$ ; and the trigger level is set at 500 mV.

### **B.1.3.1 Saving Waveforms to Floppy Diskette:**

The oscilloscope is equipped with a 3.5" floppy diskette drive allowing that waveforms and FFT spectra can be saved as computer files for use in calculations using other software packages or for later display and manipulation by the oscilloscope. It should be noted that when files (waveforms/FFT spectra) are being saved diskette, the must be saved as BINARY files IF they are to be retrieved and displayed on the oscilloscope at a later time. This information IS NOT provided in the user's manual. If the waveforms/spectra are to be saved as data files for later importation into a software package for the performance of calculations, then they should be saved in an ASCII format.

All the attenuation calculations in this study are performed in MATLAB™. Although there is a menu choice for storing files in an ASCII format suitable for MATLAB™, the files do not store correctly on diskette and MATLAB™ will encounter errors when reading the files to load them. This problem is rectified by instead choosing the MATHCAD™ ASCII file format when storing a waveform/spectrum to diskette. This format is one which, once the files are opened in the DOS EDIT file editor and the text headers are deleted leaving only data, MATLAB™ will accept without error. These minor modifications to the data files are performed after they have been saved to diskette by the oscilloscope.

The procedure for storing a waveform/spectrum to diskette, the aforementioned details notwithstanding, is described in the user's manual.

### **B.1.3.2 Oscilloscope Set up for Toneburst Measurements:**

When making toneburst measurements, the oscilloscope should be set up with a standard single channel display. The "Persistence" should be turned off, and the "Dot Join" should be turned on. The waveform intensity may be adjusted as per the comfort of the experimenter. Under the CURSOR/MEASURE option, the oscilloscope should be set to measure "Parameters" in the "Std. Voltage" mode, and the "Statistics" should be turned off. Once a signal is acquired on Channel 1, it may be shut off and the 50 sweep average of Channel 1 may be displayed by activating "TRACE A". It should be noted that the procedure for acquiring an average waveform is described in the user's manual. After an average waveform is obtained, the peak-to-peak voltage is read from the "pkpk (A)" line of the display, and recorded in the laboratory notebook. The time duration and scaling of the waveform is variable depending upon experimental conditions and user preference.

### **B.1.3.3 Oscilloscope Set up for FFT/Pulse Measurements:**

When making FFT/Pulse measurements, the oscilloscope should be set up with a four channel display, although only three of the four channels are actually used. The procedure for obtain the four channel display is described in the user's manual. The "live" time domain waveform is displayed in Channel 1. The 50 sweep average of the

“live” waveform is displayed in “TRACE A” on the second channel, and the FFT magnitude spectrum of “TRACE A” (average waveform) is displayed in “TRACE B” on the third channel. The procedure for obtaining an FFT magnitude spectrum of a waveform is also described in the user’s manual.

The frequency range of the FFT spectrum is determined by the scaling of the time domain signal. The maximum frequency of the FFT magnitude spectrum is determined the Nyquist frequency. It is not the objective of this study to make an in-depth study of signal processing, and an excellent discussion of the FFT is given by Ramirez (1985) and by the LeCroy Operator’s Manual. Suffice to say that the Nyquist frequency is equal to one half of the effective sampling frequency (after decimation), and the effective sampling frequency is determined by the scaling of the time domain waveform. It is recommended that the time domain scaling be set so that the Nyquist frequency is 5.00 MHz for the 1.0 MHz and 2.25 MHz transducers, and that the Nyquist frequency is 12.5 MHz for the 5.0 MHz, 7.5 MHz, and 10.0 MHz transducers. It should be noted that there is also a useful discussion and exercise on the use of the FFT and decimation by Dr. Margaret Greenwood of the Battelle Pacific Northwest National Laboratory beginning on page 38 of the laboratory notebook numbered APD-005. It is recommended that this discussion and exercise be studied by any user not familiar with the use of FFT’s.

It is preferable to use a rectangular sampling window for the FFT/Pulse measurements. The time domain waveform (pulse) should be centered as well as possible in the window. This should be done as the FFT algorithm assumes periodicity of the waveform, and waveform position in the window can affect FFT results (cf. Ramirez

1985). The amplitude scaling of the time domain signal should be set according to experimental conditions.

To perform the FFT analysis, a time domain waveform of the received pulse should be acquired and displayed in Channel 1. The amplitude (voltage) scaling should be adjusted, together with the attenuation settings on the Pulser/Receiver, if necessary, to obtain a distinct received pulse waveform. An average waveform should then be acquired in "TRACE A". The averages are generally performed over 50 sweeps, the number of sweeps can be changed if experimental conditions; i.e., rapidly separating systems, dictate. Once the average has been performed and displayed by the oscilloscope, the sample acquisition in the "live" waveform should be stopped by pressing the "STOP" button on the control panel of the oscilloscope. The FFT magnitude spectrum of the average waveform should be performed as described in the user's manual. Once the FFT magnitude spectrum has been acquired, the spectrum should be saved to diskette in an ASCII MATHCAD™ format as described in Section B.1.3.1. It should be noted that a "hard copy" of the oscilloscope display should be made by pressing the "SCREEN DUMP" button on the control panel of the oscilloscope.

#### **B.1.4 Operation of the Photomicrographic Video Imaging System:**

Bubble size measurements and volume fraction estimates are obtained by using the video imaging system described in Section 3.1.3. Video Images are obtained using the Company 7 "Questar" QM-100 long distance microscope which is coupled, as a single unit, to a Cohu Model 4810 monochrome CCD video camera. There is a user's

manual for both the microscope and video camera available in the laboratory which describe procedures as to the care and maintenance of these instruments. It should be noted that the camera is "on" whenever the AC power adapter is plugged in. The microscope/camera unit is mounted on a sliding track which allows for variability of the working distance; i.e., the distance between the microscope objective and object to be studied. In the experiments performed in this study, it was found that a working distance of 17.8 cm (7") allowed for the widest range of bubble size measurements without changing the focus of the microscope. Achieving the widest range of measurements is important in that any time the focus or working of the microscope is changed, the calibration must be performed to reset the pixel to distance scale in the image analysis software.

Backlighting is provided by a strobotach directly behind the sample cell at a distance of 61 cm (24"). The strobotach is synchronized to the video camera via the wire lead protruding from the back of the camera. This wire is connected to the vertical update "pin" on the "U8" integrated circuit chip in the camera. The schematic diagram of this chip is available in the laboratory in the Installation and Operation Instructions manual for the camera. The synchronization lead wire is connected by a coaxial cable to the "GATE/TRIG IN" connector on the Global Specialties Corporation 40001 Pulse Generator. The pulse generator is used to trigger the strobotach. The vertical update signal from the camera has a frequency which is actually twice the frame/second rate of the camera. The camera updates at twice the frame/second rate because the odd numbered lines on the CCD chip are acquired first, then the even numbered lines are

“filled in”. Therefore, the vertical update rate of the camera (60 Hz) is twice the frame/second rate (30 Hz), and the vertical update signal must be effectively divided by two by the pulse generator in order to synchronize the strobotach such that moving bubbles will be “frozen” in the acquired images. The pulse generator is then connected to the strobotach by connecting the “VAR OUT” connector on the pulse generator, via coaxial cable, to the “INPUT” connector on the strobotach. The amplitude of the pulse generator signal should be adjusted, by trial and error, to be sufficient in amplitude to trigger the strobotach.

Calibration of the microscope/camera unit must be performed each time the focus or working distance of the microscope is changed. This calibration is performed using a reticle mounted on a Plexiglas plate. The reticle has a series of linear and circular scales the dimensions of which are marked on the reticle. The reticle is rated by the manufacturer (Edmund Scientific Company, Barrington, NJ) to be accurate to within 2  $\mu\text{m}$ . Calibration is performed by immersing the reticle in the liquid in which the sample is suspended. The focus is set so that the image of the reticle is as clear as possible, and then the focus is NOT to be changed during bubble measurements without recalibrating. It is preferable to focus on the 0.005” (127  $\mu\text{m}$ ) circle on the reticle as it is the smallest calibration feature. Once the image is focused, a one or two frame “movie” should be acquired using the image analysis software and saved to be added to stacks of movie frames of bubbles (the procedure for making movies will be discussed in the next paragraph). An example image of the reticle used in calibration is shown in Figure B.1.

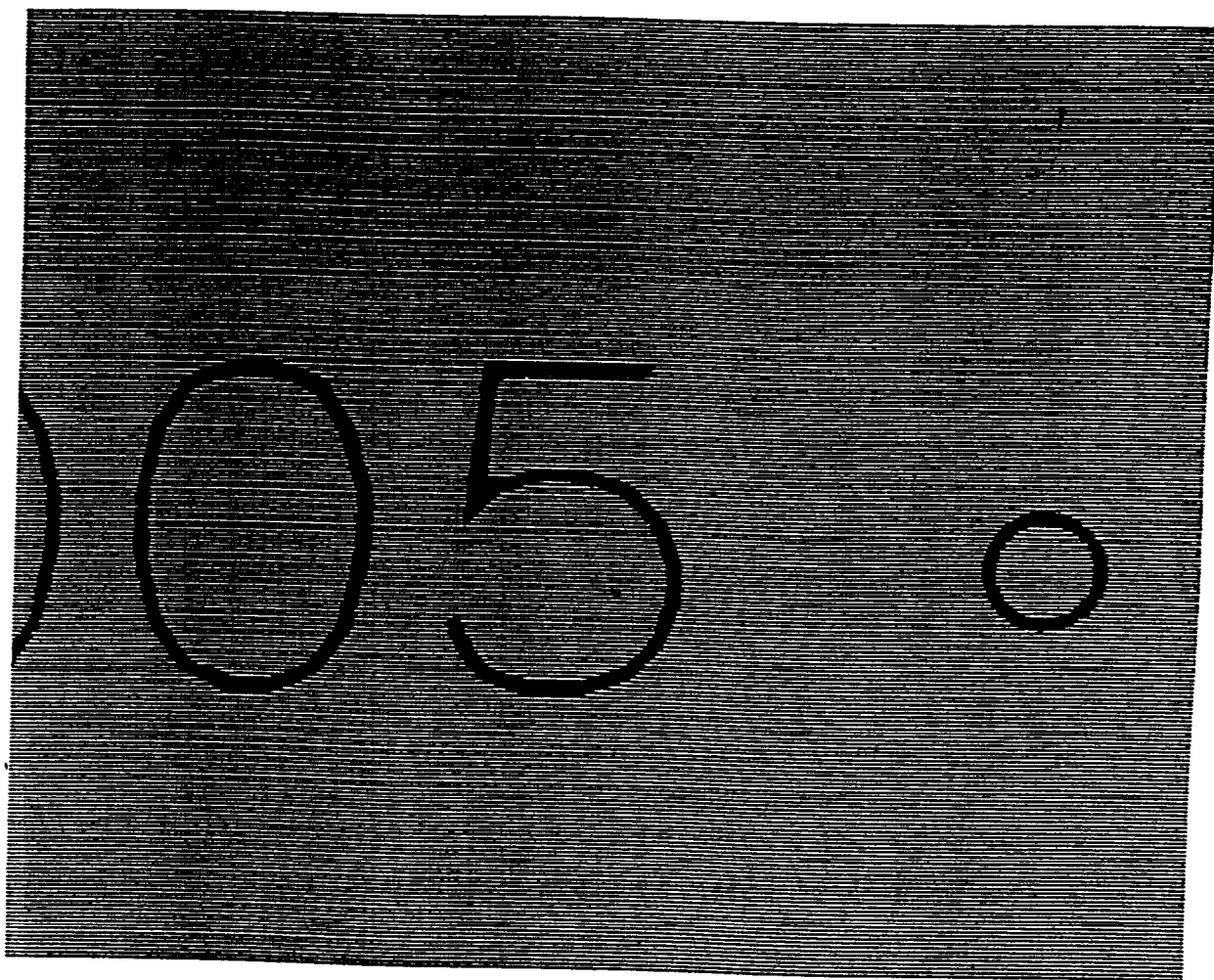


Figure B.1: Photograph of the 0.005" diameter circle on the reticle used in calibrating the photomicrographic video imaging system.

The movie frames containing the reticle image will then be measured to set the pixel to length scale in the image analysis software.

The images acquired by the microscope/camera unit are analyzed using the *Image SXM* image analysis software package installed on the Apple Power Macintosh G3 computer which is interfaced with the microscope/camera unit. The *Image SXM* image analysis software package does not have a user's manual *per se*, but it is almost identical to the *NIH Image* image analysis software package available through the National Institutes of Health. The *NIH Image* image analysis software package has an online manual available at the NIH Internet site at <http://rsb.info.nih.gov/nih-image/manual/Contents.html>. Images are obtained by opening *Image SXM* on the desktop of the Power Macintosh. When the *Image SXM* folder opens, open the program by double clicking on the *Image SXM* icon. When the program is open, a live video image can be obtained by clicking on the "Special" menu choice and choosing the "Start Capturing" option. Movies are acquired by selecting the entire image screen and then choosing the "Stacks" menu choice. Choose "Make Movie" option and follow the menu options which appear. It is usually desirable to acquire about 40 frames in each movie, but this number can be adjusted to match experimental conditions. An example bubble image is shown in Figure B.2. The details of these procedures are described in the online manual, and the manual should be examined by user's not familiar with this software package.

When a movie has been acquired, frames which do not have any images should be deleted from the "stack" as per the user's manual to conserve disk space on the computer.

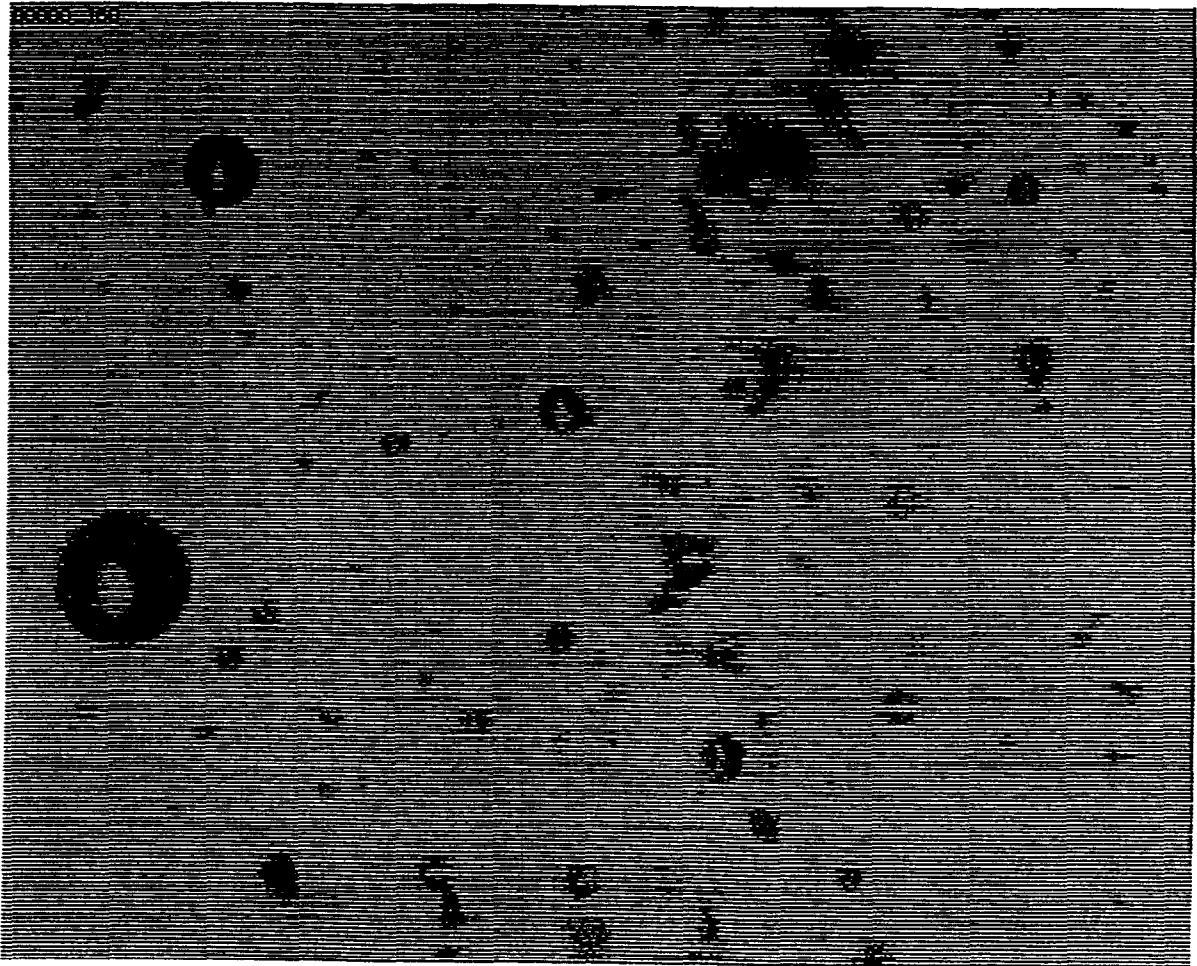
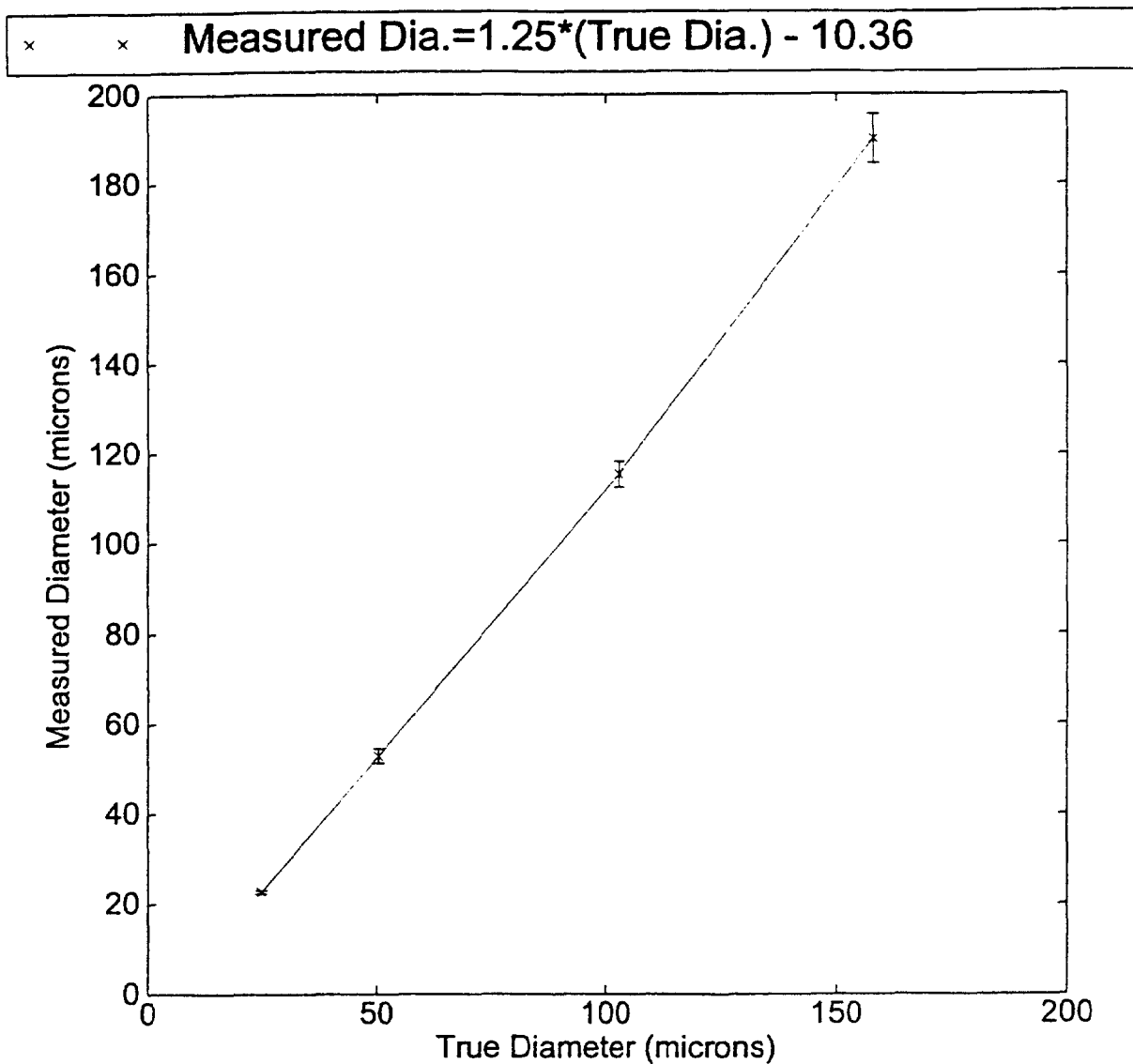


Figure B.2: Photograph of a electrolytically generated "bubble stream". The bubbles are generated at 40 V, 6 to 8 mA, <1 W.

Also, the image frames of the reticle should be added to the image stack and saved with the movie. Calibration is performed by using the straight line tool to draw a diameter across the reticle circle. Then choose the “Analyze” menu choice and choose the “Set Scale” option. Enter the known distance in the appropriate units and click on the “OK” choice. The pixel to length scale is now set. It is usually a good idea to measure the reticle circle diameter vertically, horizontally, and on each diagonal and average the reported pixel/ $\mu\text{m}$  conversion factor to be used in scaling. This average value can then be entered manually in the set scale procedure instead of the known distance of the reticle diameter.

Once the scale has been set, size measurements can be made on images by using a similar technique. The straight line tool is used to draw a diameter across a bubble of interest, and the “Analyze” menu choice is chosen. Now the “Measure” option should be chosen and the length of the line drawn will be displayed in microns in the “Info” display box. The measurement should be recorded. Measurement should only be made on bubbles which are in focus and are not touching other bubbles or the edge of the image frame. The backlighting will cause some error due to shadowing in the bubble size measurement. Therefore, a calibration curve of measured versus true size of polystyrene optical standard particles is shown in Figure B.3.

One set of bubble size measurements is performed for bubbles generated in water both by electrolysis and aeration. Photographs are made of these bubbles using the above technique, and size measurements are performed using the above procedure. The results of these measurements are used to estimate a bubble size distribution for bubbles generated



**Figure B.3:** Calibration plot relating measured particle diameters to the NIST certified diameters of polystyrene particle standards.

electrolytically at 40 V; 6 to 8 mA; < 1W. This size distribution is determined to have a mean diameter of 51  $\mu\text{m}$  and a standard deviation of 26  $\mu\text{m}$ . A log-normal size distribution is fitted to these data, and the results are shown in Figure B.4.

Volume fraction estimation is obtained from knowledge of the field of view and depth of field of the microscope at a particular working distance, and the number of bubbles in a given frame averaged over the number of frames in the movie stack. This estimation, of course, assumes that the bubbly liquid is well mixed, and the image field is representative of conditions throughout the sample cell.

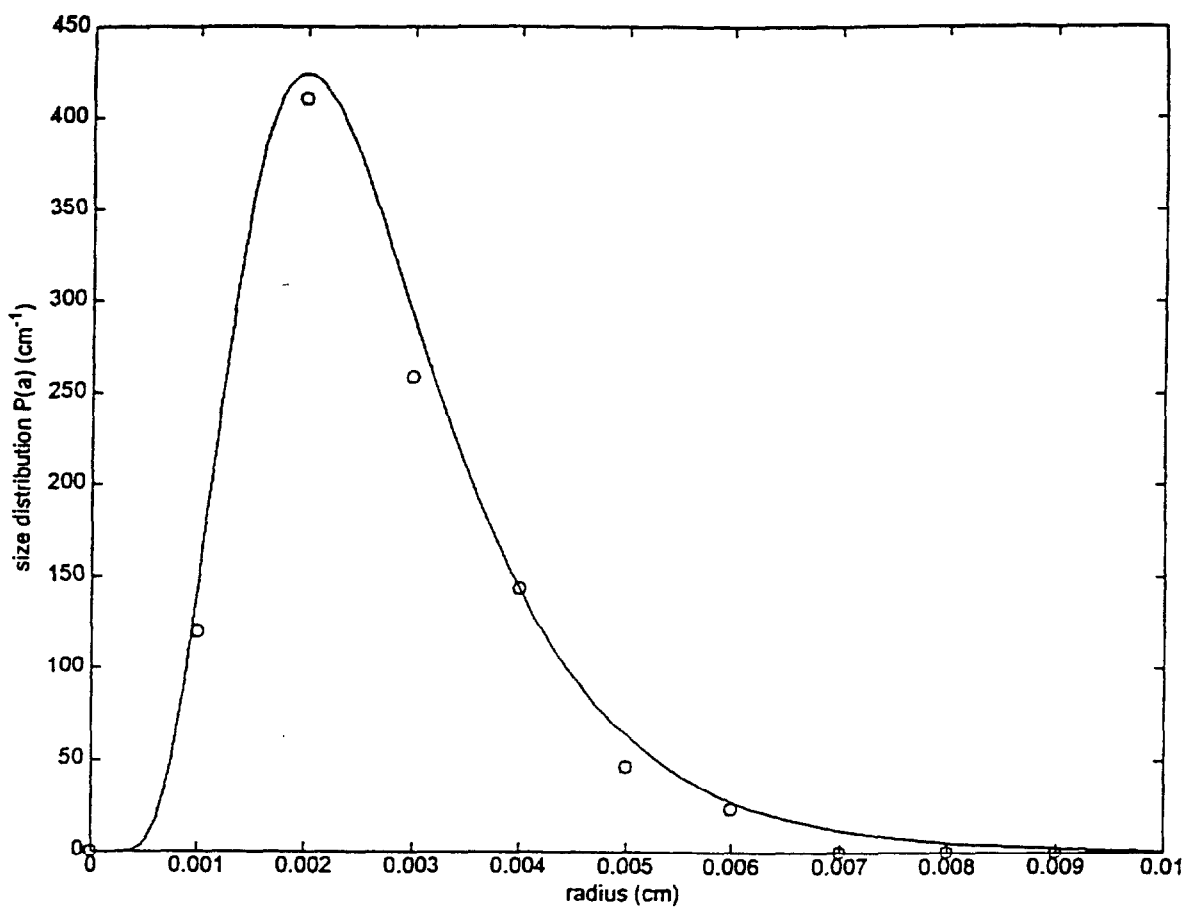


Figure B.4: Bubble size distribution determined by the microphotographic video imaging system and the log-normal size distribution fitted to the data.

## Appendix C: MATLAB™ Routines

The following pages contain some of the various MATLAB™ routines used to calculate attenuation from raw voltage data in slurries and then plot calculated attenuation as either a function of frequency or solids concentration.

Not all the existing MATLAB™ routines are shown in this appendix. The reason for this is because many of the routines are simply variations of one-another. Therefore, for the sake of brevity, only the most important “watershed” routines, upon which all the others are derived, are shown.

The routines are annotated with comment lines to explain the progression of data manipulation within the routines. Each version of MATLAB™ is provided with a user's manual, and the later versions available in our laboratories also have on-line help through Netscape™. The User's Guide (black cover book) from the earliest version (v.4.2c.1) of MATLAB™ is available in the laboratory. Although, new versions of MATLAB™ have been installed on the laboratory computers, this user's manual contains a tutorial on the basic functions and capabilities of MATLAB™. It is recommended that anyone who is not familiar with MATLAB™ take the time to read and follow the tutorial to gain experience in using this software package.

```
%This program calculates attenuation vs frequency in slurries of  
%Soda-lime glass beads using Direct  
%(Toneburst) Oscilloscope Data  
%(called DIRECT.m)
```

```
%Load 0.5 MHz water data  
load s1wdp5.dat  
fwp5=[s1wdp5(:,1)];  
vwp5=[s1wdp5(:,2)];
```

```
%Load 0.5 MHz slurry data  
load s1sdp5.dat  
fsp5=[s1sdp5(:,1)];  
vsp5=[s1sdp5(:,2)];
```

```
%Load 1.0 MHz water data  
load s1wd1.dat  
fw1=[s1wd1(:,1)];  
vw1=[s1wd1(:,2)];
```

```
%Load 1.0 MHz slurry data  
load s1sd1.dat  
fs1=[s1sd1(:,1)];  
vs1=[s1sd1(:,2)];
```

```
%Load 2.25 MHz water data  
load s1wd2.dat  
fw2=[s1wd2(:,1)];  
vw2=[s1wd2(:,2)];
```

```
%Load 2.25 MHz slurry data  
load s1sd2.dat  
fs2=[s1sd2(:,1)];  
vs2=[s1sd2(:,2)];
```

```
%Load 5.0 MHz water data  
load s1wd5.dat  
fw5=[s1wd5(:,1)];  
vw5=[s1wd5(:,2)];
```

```
%Load 5.0 MHz slurry data  
load s1sd5.dat  
fs5=[s1sd5(:,1)];  
vs5=[s1sd5(:,2)];
```

```
%Load 7.5 MHz water data
load slwd7.dat
fw7=[slwd7(:,1)];
vw7=[slwd7(:,2)];

%Load 7.5 MHz slurry data
load slsd7.dat
fs7=[slsd7(:,1)];
vs7=[slsd7(:,2)];

%Load 10.0 MHz water data
load slwd10.dat
fw10=[slwd10(:,1)];
vw10=[slwd10(:,2)];

%Load 10.0 MHz slurry data
load slsd10.dat
fs10=[slsd10(:,1)];
vs10=[slsd10(:,2)];

%Input Transducer Separation Distances in cm
dp5=4.006*2.54;
d1=4.006*2.54;
d2=3.9875*2.54;
d5=4.072*2.54;
d7=1.986*2.54;
d10=2.040*2.54;

%Calculate Slurry to Water voltage ratios
vrp5=vsp5./vwp5;
vr1=vs1./vw1;
vr2=vs2./vw2;
vr5=vs5./vw5;
vr7=vs7./vw7;
vr10=vs10./vw10;

%Calculate logs of voltage ratios
lvrp5=log10(vrp5);
lvr1=log10(vr1);
lvr2=log10(vr2);
lvr5=log10(vr5);
lvr7=log10(vr7);
```

```

lvr10=log10(vr10);

%Calculate attenuation
ap5=-1.0*(lvrp5/dp5)
a1=-1.0*(lvr1/d1)
a2=-1.0*(lvr2/d2)
a5=-1.0*(lvr5/d5)
a7=-1.0*(lvr7/d7)
a10=-1.0*(lvr10/d10)

%Rectify with theory (put in Np/cm using natural logarithms)
ap5=ap5*2.302;
a1=a1*2.302;
a2=a2*2.302;
a5=a5*2.302;
a7=a7*2.302;
a10=a10*2.302;

%Use one set of frequencies per transducer to plot
fp5=fwp5;
f1=fw1;
f2=fw2;
f5=fw5;
f7=fw7;
f10=fw10;

%Convert Frequency into Hz
fp5=1.0e6*fp5
f1=1.0e6*f1
f2=1.0e6*f2
f5=1.0e6*f5
f7=1.0e6*f7
f10=1.0e6*f10

%Plot results
loglog(fp5,ap5,':')
%title('Direct Oscilloscope Measurements-5% glass (5 micron)')
ylabel('Attenuation (dB/cm)')
xlabel('Frequency (Hz)')
hold on
loglog(f1,a1,':')
hold on
loglog(f2,a2,':')
hold on

```

```

loglog(f5,a5,'')
hold on
loglog(f7,a7,'')
hold on
loglog(f10,a10,'')
hold on

```

```

***** END OF DIRECT.M*****

```

```

%Program to plot average attenuation vs concentration at various fixed
%frequencies for Dense Potters Beads Slurries in Glycerol/water Mixture
%(Called AVSPHI.m)

```

```

%Concentration (volume fraction) arrays

```

```

c1p5=[0.05 0.10 0.15 0.20 0.30 0.40 0.45 0.50];%f=1.5 MHz
c1p75=[0.05 0.10 0.15 0.20 0.30 0.40 0.45 0.50];%f=1.75 MHz
c2=[0.05 0.10 0.15 0.20 0.30 0.40 0.45 0.50];%f=2.0 MHz
c2p25=[0.05 0.10 0.15 0.20 0.30 0.40 0.45 0.50];%2.25 MHz
c2p5=[0.05 0.10 0.15 0.20 0.30 0.40 0.45 0.50];%f=2.5 MHz
c2p75=[0.05 0.10 0.15 0.20 0.30 0.40 0.45 0.50];%f=2.75 MHz
c3=[0.05 0.10 0.15 0.20 0.30 0.40 0.45 0.50];%f=3.0 MHz
c3p5=[0.05 0.10 0.15 0.20 0.30 0.40 0.45 0.50];%f=3.5 MHz
c4=[0.05 0.10 0.15 0.20 0.30 0.40 0.45 0.50];%f=4.0 MHz
c4p5=[0.05 0.10 0.15 0.20 0.30 0.40 0.45 0.50];%f=4.5 MHz
c5=[0.05 0.10 0.15 0.20 0.30 0.45 0.50];%f=5.0 MHz

```

```

%Attenuation Arrays--Attenuations are average values at freqs. where transducers
%overlap and data from multiple experiments is available.

```

```

a1p5=[0.0388 0.0578 0.0839 0.111 0.148 0.149 0.189 0.281];
a1p75=[0.0436 0.0833 0.119 0.152 0.203 0.202 0.257 0.411];
a2=[0.0731 0.122 0.160 0.205 0.240 0.243 0.303 0.437];
a2p25=[0.0794 0.164 0.232 0.299 0.361 0.318 0.350 0.486];
a2p5=[0.135 0.232 0.319 0.393 0.502 0.449 0.431 0.459];
a2p75=[0.144 0.310 0.426 0.528 0.664 0.598 0.540 0.572];
a3=[0.195 0.414 0.543 0.660 0.847 0.778 0.792 0.748];
a3p5=[0.321 0.596 0.679 0.872 1.20 1.36 1.40 1.28];
a4=[0.469 0.961 1.16 1.65 2.33 2.19 2.37 2.21];
a4p5=[0.613 1.16 1.56 2.44 3.32 2.91 3.57 3.74];
a5=[0.887 1.39 2.23 3.09 3.89 4.70 5.94];

```

```

%Plot Results

```

```

semilogy(c1p5,a1p5,'r-')

```

```

hold on
axis([0.0 0.6 0.0 6.0])
semilogy(c1p75,a1p75,'r-')
hold on
semilogy(c2,a2,'r-')
hold on
semilogy(c2p25,a2p25,'r-')
hold on
semilogy(c2p5,a2p5,'r-')
hold on
semilogy(c2p75,a2p75,'r-')
hold on
semilogy(c3,a3,'r-')
hold on
xlabel('Solids Volume Fraction')
ylabel('Attenuation (Np/cm)')
hold on
semilogy(c3p5,a3p5,'y-')
hold on
semilogy(c4,a4,'y-')
hold on
semilogy(c4p5,a4p5,'y-')
hold on
semilogy(c5,a5,'y-')
hold on

```

\*\*\*\*\*END OF AVSPHI.DOC\*\*\*\*\*

```

%Program to calculate attenuation by FFT
%of three phase systems of soda lime glass beads
%in water at vol. fract.~ 0.10
%with air generated bubbles at 100 ml/min (called sgl1.m)

```

```

%Load FFT magnitude data files
%Load 5 MHz water data
load cont5w.dat
%choose only the frequencies in the effective x-ducer operating range
%and disregard the rest..do for all x-ducer pairs.
n5w=max(size(cont5w));
fw5=[cont5w(0.20*n5w:0.5*n5w,1)];
v5wag=[cont5w(0.20*n5w:0.5*n5w,2)];

```

```

%Load 5 MHz slurry w/out bubbles data

```

```
load cont5s.dat
n5s=max(size(cont5s));
fs5=[cont5s(0.20*n5s:0.5*n5s,1)];
v5sag=[cont5s(0.20*n5s:0.5*n5s,2)];

%Load 5 MHz slurry w/ bubble data
load cont5b.dat
n5b=max(size(cont5b));
fs5b=[cont5b(0.20*n5b:0.5*n5b,1)];
v5sagb=[cont5b(0.20*n5b:0.5*n5b,2)];

%Load 2.25 MHz water data
load cont2w.dat
n2w=max(size(cont2w));
fw2=[cont2w(0.25*n2w:0.5*n2w,1)];
v2wag=[cont2w(0.25*n2w:0.5*n2w,2)];

%Load 2.25 MHz slurry w/out bubbles data
load cont2s.dat
n2s=max(size(cont2s));
fs2=[cont2s(0.25*n2s:0.5*n2s,1)];
v2sag=[cont2s(0.25*n2s:0.5*n2s,2)];

%Load 2.25 MHz slurry with bubble bubble data
load cont2b.dat
n2b=max(size(cont2b));
fs2b=[cont2b(0.25*n2b:0.5*n2b,1)];
v2bag=[cont2b(0.25*n2b:0.5*n2b,2)];

%Load 1.0 MHz water data
load cont1w.dat
n1w=max(size(cont1w));
fw1=[cont1w(0.14*n1w:0.25*n1w,1)];
v1wag=[cont1w(0.14*n1w:0.25*n1w,2)];

%Load 1.0 MHz slurry w/out bubbles data
load cont1s.dat
n1s=max(size(cont1s));
fs1=[cont1s(0.14*n1s:0.25*n1s,1)];
v1sag=[cont1s(0.14*n1s:0.25*n1s,2)];

%Load 1.0 MHz bubble data
load cont1b.dat
n1b=max(size(cont1b));
```

```

fs1b=[cont1b(0.14*n1b:0.25*n1b,1)];
v1bag=[cont1b(0.14*n1b:0.25*n1b,2)];

%Load 0.5 MHz water data
load thruyp5w.dat
np5w=max(size(thruyp5w));
fwp5=[thruyp5w(0.03*np5w:0.07*np5w,1)];
vp5wag=[thruyp5w(0.03*np5w:0.07*np5w,2)];

%Load 0.5 MHz slurry w/out bubbles data
load thruyp5s.dat
np5s=max(size(thruyp5s));
fsp5=[thruyp5s(0.03*np5s:0.07*np5s,1)];
vp5sag=[thruyp5s(0.03*np5s:0.07*np5s,2)];

%Load 0.5 MHz slurry with bubble bubble data
load thruyp5b.dat
np5b=max(size(thruyp5b));
fsp5b=[thruyp5b(0.03*np5b:0.07*np5b,1)];
vp5bag=[thruyp5b(0.03*np5b:0.07*np5b,2)];

%Load 7.5 MHz water data
load cont7w.dat
n7w=max(size(cont7w));
fw7=[cont7w(0.3*n7w:0.4*n7w,1)];
v7wag=[cont7w(0.3*n7w:0.4*n7w,2)];

%Load 7.5 MHz slurry w/out bubbles data
load cont7s.dat
n7s=max(size(cont7s));
fs7=[cont7s(0.3*n7s:0.4*n7s,1)];
v7sag=[cont7s(0.3*n7s:0.4*n7s,2)];

%Load 7.5 MHz slurry w/ bubble data
load cont7b.dat
n7b=max(size(cont7b));
fs7b=[cont7b(0.3*n7b:0.4*n7b,1)];
v7sagb=[cont7b(0.3*n7b:0.4*n7b,2)];

%Load 10 MHz water data
load cont10w.dat
n10w=max(size(cont10w));
fw10=[cont10w(0.35*n10w:0.8*n10w,1)];
v10wag=[cont10w(0.35*n10w:0.8*n10w,2)];

```

```

%Load 10 MHz polysty slurry w/out bubbles data
load cont10s.dat
n10s=max(size(cont10s));
fs10=[cont10s(0.35*n10s:0.8*n10s,1)];
v10sag=[cont10s(0.35*n10s:0.8*n10s,2)];

%Load 10 MHz slurry w/ bubble data
load cont10b.dat
n10b=max(size(cont10b));
fs10b=[cont10b(0.35*n10b:0.8*n10b,1)];
v10sagb=[cont10b(0.35*n10b:0.8*n10b,2)];

%Correct Voltage Values for Receiver Attenuation and gain
v5wg=v5wag./(10.^((40-54)/20));
v5sbg=v5sagb./(10.^((40-46)/20));
v2sg=v2sag./(10.^((40-44)/20));
v2bg=v2bag./(10.^((40-44)/20));
v5sg=v5sag./(10.^((40-46)/20));
v2wg=v2wag./(10.^((40-46)/20));
v1wg=v1wag./(10.^((40-50)/20));
v1sg=v1sag./(10.^((40-50)/20));
v1bg=v1bag./(10.^((40-50)/20));
vp5wg=vp5wag./(10.^((40-46)/20));
vp5sg=vp5sag./(10.^((40-46)/20));
vp5bg=vp5bag./(10.^((40-46)/20));
v7wg=v7wag./(10.^((40-48)/20));
v7sbg=v7sagb./(10.^((40-34)/20));
v7sg=v7sag./(10.^((40-34)/20));
v10wg=v10wag./(10.^((40-38)/20));
v10sbg=v10sagb./(10.^((40-24)/20));
v10sg=v10sag./(10.^((40-24)/20));

%Renaming variables to be less confusing
v5w=v5wg;
v5sb=v5sbg;
v2s=v2sg;
v2b=v2bg;
v5s=v5sg;
v2w=v2wg;
v1w=v1wg;
v1s=v1sg;
v1b=v1bg;
vp5w=vp5wg;

```

```
vp5s=vp5sg;  
vp5b=vp5bg;  
v7w=v7wg;  
v7sb=v7sgb;  
v7s=v7sg;  
v10w=v10wg;  
v10sb=v10sgb;  
v10s=v10sg;
```

```
%Voltage ratios  
vr2b=v2b./v2w;  
vr5b=v5sb./v5w;  
vr2s=v2s./v2w;  
vr5s=v5s./v5w;  
vr1s=v1s./v1w;  
vr1b=v1b./v1w;  
vrp5s=vp5s./vp5w;  
vrp5b=vp5b./vp5w;  
vr7b=v7sb./v7w;  
vr7s=v7s./v7w;  
vr10b=v10sb./v10w;  
vr10s=v10s./v10w;
```

```
%Log of Ratios  
lvr2b=log(vr2b);  
lvr5b=log(vr5b);  
lvr2s=log(vr2s);  
lvr5s=log(vr5s);  
lvr1s=log(vr1s);  
lvr1b=log(vr1b);  
lvrp5s=log(vrp5s);  
lvrp5b=log(vrp5b);  
lvr7b=log(vr7b);  
lvr7s=log(vr7s);  
lvr10b=log(vr10b);  
lvr10s=log(vr10s);
```

```
%Transducer Separation Distances in cm  
d5=2.014*2.54;  
d2=1.982*2.54;  
d1=1.984*2.54;  
dp5=4.7;  
d7=1.717*2.54;  
d10=1.704*2.54;
```

```

%Calculate Attenuation
as2b=-1.0.*(lvr2b./d2);
as5s=-1.0.*(lvr5s./d5);
as2s=-1.0.*(lvr2s./d2);
as5b=-1.0.*(lvr5b./d5);
as1s=-1.0.*(lvr1s./d1);
as1b=-1.0.*(lvr1b./d1);
asp5s=-1.0.*(lvrp5s./dp5);
asp5b=-1.0.*(lvrp5b./dp5);
as7s=-1.0.*(lvr7s./d7);
as7b=-1.0.*(lvr7b./d7);
as10s=-1.0.*(lvr10s./d10);
as10b=-1.0.*(lvr10b./d10);

%Normalize attenuation by f^2
%as2b=as2b./(fs2b.^2);
%as5s=as5s./(fw5.^2);
%as2s=as2s./(fs2.^2);
%as5b=as5b./(fs5b.^2);
%as1s=as1s./(fs1.^2)
%as1b=as1b./(fs1b.^2)
%asp5s=asp5s./(fsp5.^2)
%asp5b=asp5b./(fsp5b.^2)
%as7s=as7s./(fw7.^2);
%as7b=as7b./(fs7b.^2);
%as10s=as10s./(fw10.^2);
%as10b=as10b./(fs10b.^2);

%Use one set of frequencies per transducer to make plots
f5=fw5;
f5b=fs5b;
f2=fs2;
f2b=fs2b;
f1=fs1;
f1b=fs1b;
fp5=fsp5;
fp5b=fsp5b;
f7=fw7;
f7b=fs7b;
f10=fw10;
f10b=fs10b;

%Plot Results

```

```

loglog(f2,as2s,'w+')
hold on
loglog(f2b,as2b,'w-')
hold on
loglog(f5,as5s,'r+')
hold on
loglog(f5b,as5b,'r-')
hold on
loglog(f1,as1s,'g+')
hold on
loglog(f1b,as1b,'g-')
hold on
%loglog(fp5,asp5s,'b+')
hold on
%loglog(fp5b,asp5b,'b-')
hold on
loglog(f7,as7s,'g+')
hold on
loglog(f7b,as7b,'b-')
hold on
loglog(f10,as10s,'y+')
hold on
loglog(f10b,as10b,'b-')
hold on
%axis([1.0e6 1.0e7 1.0e-17 1.0e-13])
title('Attenuation Results')
xlabel('Frequency (Hz)')
ylabel('Attenuation (Np/cm)')
%loglog(f10r,as10r,'ro')
hold on

*****END OF SGL1.M*****

%Program to calculate attenuation by FFT
%of a5% Solution
%(158 micron diameter polystyrene beads)
% 2" in plexiglas test cell
%This program plots FFT and toneburst results
%(called STYRENE5.m)

%Load 0.5 MHz water data
%load s3wp5.dat
%fwp5=[s3wp5(:,1)];
%dbmp5w=[s3wp5(:,2)];

```

```
%Load 0.5 MHz slurry data
%load s3sp5.dat
%fsp5=[s3sp5(:,1)];
%dbmp5s=[s3sp5(:,2)];

%Load 1.0 MHz water data
load sty51w.dat
n1w=max(size(sty51w));
fw1=[sty51w(0.18*n1w:0.3*n1w,1)];
v1wag=[sty51w(0.18*n1w:0.3*n1w,2)];

%Load 1.0 MHz slurry data
load sty51s.dat
n1s=max(size(sty51s));
fs1=[sty51s(0.18*n1s:0.3*n1s,1)];
v1sag=[sty51s(0.18*n1s:0.3*n1s,2)];

%Load 2.25 MHz water data
load sty52w.dat
n2w=max(size(sty52w));
fw2=[sty52w(0.3*n2w:0.5*n2w,1)];
v2wag=[sty52w(0.3*n2w:0.5*n2w,2)];

%Load 2.25 MHz slurry data
load sty52s.dat
n2s=max(size(sty52s));
fs2=[sty52s(0.3*n2s:0.5*n2s,1)];
v2sag=[sty52s(0.3*n2s:0.5*n2s,2)];

%Load 5.0 MHz water data
load sty55w.dat
n5w=max(size(sty55w));
fw5=[sty55w(0.25*n5w:0.5*n5w,1)];
v5wag=[sty55w(0.25*n5w:0.5*n5w,2)];

%Load 5.0 MHz slurry data
load sty55s.dat
n5s=max(size(sty55s));
fs5=[sty55s(0.25*n5s:0.5*n5s,1)];
v5sag=[sty55s(0.25*n5s:0.5*n5s,2)];

%Load 5.0 MHz (repeat) water data
%load sty55w.dat
```

```

%n5wr=max(size(sty55w));
%fw5r=[tc305wr(0.25*n5wr:0.5*n5wr,1)];
%v5wagr=[tc305wr(0.25*n5wr:0.5*n5wr,2)];

```

```

%Load 5.0 MHz (repeat) slurry data
%load tc305sr.dat
%n5sr=max(size(tc305sr));
%fs5r=[tc305sr(0.25*n5sr:0.5*n5sr,1)];
%v5sagr=[tc305sr(0.25*n5sr:0.5*n5sr,2)];

```

```

%Load 7.5 MHz water data
load sty57w.dat
n7w=max(size(sty57w));
fw7=[sty57w(0.40*n7w:0.80*n7w,1)];
v7wag=[sty57w(0.40*n7w:0.80*n7w,2)];

```

```

%Load 7.5 MHz slurry data
load sty57s.dat
n7s=max(size(sty57s));
fs7=[sty57s(0.40*n7s:0.80*n7s,1)];
v7sag=[sty57s(0.40*n7s:0.80*n7s,2)];

```

```

%Load 10.0 MHz water data
load sty510w.dat
n10w=max(size(sty510w))
fw10=[sty510w(0.60*n10w:0.98*n10w,1)];
v10wag=[sty510w(0.60*n10w:0.98*n10w,2)];

```

```

%Load 10.0 MHz slurry data
load sty510s.dat
n10s=max(size(sty510s));
fs10=[sty510s(0.60*n10s:0.98*n10s,1)];
v10sag=[sty510s(0.60*n10s:0.98*n10s,2)];

```

```

%Correct Voltages for Receiver Attenuation and gain
v1wg=v1wag./(10.^((40-52)/20));
v7wg=v7wag./(10.^((40-48)/20));
v5wg=v5wag./(10.^((40-44)/20));
%vp5wg=vp5wag./(10.^((40-36)/20));
v2wg=v2wag./(10.^((40-52)/20));
%v5wgr=v5wagr./(10.^((40-50)/20));
v10wg=v10wag./(10.^((40-40)/20));
%v10wgr=v10wagr./(10.^((40-40)/20));

```

```

v1sg=v1sag./(10.^((40-52)/20));
v7sg=v7sag./(10.^((40-28)/20));
v5sg=v5sag./(10.^((40-30)/20));
%vp5sg=vp5sag./(10.^((40-36)/20));
v2sg=v2sag./(10.^((40-52)/20));
%v5sgr=v5sagr./(10.^((40-10)/20));
v10sg=v10sag./(10.^((40-20)/20));
%v10sgr=v10sagr./(10.^((40-10)/20));

```

```

%Renaming variables to be less confusing

```

```

v1w=v1wg;
v7w=v7wg;
v5w=v5wg;
%vp5w=vp5wg;
v2w=v2wg;
%v5wr=v5wgr;
v10w=v10wg;
%v10wr=v10wgr;

```

```

v1s=v1sg;
v7s=v7sg;
v5s=v5sg;
%vp5s=vp5sg;
v2s=v2sg;
%v5sr=v5sgr;
v10s=v10sg;
%v10sr=v10sgr;

```

```

%Voltage ratios

```

```

vr1=v1s./v1w
vr7=v7s./v7w;
vr5=v5s./v5w;
%vrp5=vp5s./vp5w;
vr2=v2s./v2w;
%vr5r=v5sr./v5wr;
vr10=v10s./v10w;
%vr10r=v10sr./v10wr;

```

```

%Log of Ratios

```

```

lvr1=log10(vr1)
lvr7=log10(vr7);
lvr5=log10(vr5);
%lvrp5=log10(vrp5);
lvr2=log10(vr2);

```

```

%lvr5r=log10(vr5r);
lvr10=log10(vr10);
%lvr10r=log10(vr10r);

%Transducer Separation Distances in cm
%dp5=4.941*2.54;
d1=2.008*2.54
d2=1.995*2.54;
%d5r=1.998*2.54;
d5=1.995*2.54;
d7=1.719*2.54;
d10=1.700*2.54;
%d10r=1.770*2.54;

%Calculate Attenuation
as1=-1.0.*(lvr1./d1);
as7=-1.0.*(lvr7./d7);
as5=-1.0.*(lvr5./d5);
%asp5=-1.0.*(lvrp5./dp5);
as2=-1.0.*(lvr2./d2);
%as5r=-1.0.*(lvr5r./d5r);
as10=-1.0.*(lvr10./d10);
%as10r=-1.0.*(lvr10r./d10r);

%Multiply by 2.302 to rectify with natural log calculation, i.e. put in Np/cm
as1=2.302.*as1
as7=2.302.*as7;
as5=2.302.*as5;
%asp5=2.302.*asp5
as2=2.302.*as2
%as5r=2.302.*as5r;
as10=2.302.*as10;
%as10r=2.302.*as10r;

%Use one set of frequencies per transducer to make plots
%fp5=fwp5;
f1=fw1;
f2=fw2;
f5=fw5
f7=fw7;
f10=fw10;
%f5r=fw5r;
%f10r=fw10r;

```

```

%Load simulation data
load theo.dat
ff=[theo(:,1)];
af=[theo(:,2)];
%ff=ff*1.0e6;

%Toneburst results (for comparison) entered as arrays. The "fb#" stands for
%Frequency of toneBurst for # MHz transducer. The "ab#" stands for Attenuation
%of toneBurst for # MHz transducer.
fb=[3.0e6 3.2e6 3.25e6 3.3e6 3.4e6 3.5e6 3.6e6 3.7e6 3.75e6 3.8e6 3.9e6 4.2e6];
ab=[0.15 0.211 0.228 0.256 0.331 0.429 0.636 0.9197 1.22 1.200 1.53 1.84];
fb2=[0.65e6 0.70e6 0.75e6 0.80e6 0.85e6 0.90e6 0.95e6 1.0e6 1.05e6 1.10e6 1.15e6
1.20e6];
ab2=[0.0123 0.0101 0.00943 0.0133 0.0260 0.0103 0.00963 0.0128 0.00327 0.00508
0.00884 0.00696];
fb3=[3.00e6 3.25e6 3.50e6 3.75e6 3.80e6 3.85e6 3.90e6 3.95e6];
ab3=[0.1714 0.2607 0.3502 1.402 1.6517 2.1846 2.6537 2.9089];
fb4=[4.60 4.65 4.70 4.75 4.80 4.85 4.90 4.95 5.00 5.05 5.10 5.15 5.20 5.25 5.30 5.35 5.40
5.45 5.50 5.55 5.60 5.65 5.70 5.75 5.80 5.85 5.90 5.95 6.00 6.05 6.10 6.15 6.20];
fb4=fb4*1.0e6;
ab4=[4.56 4.45 4.81 4.78 4.68 4.76 4.68 4.15 3.87 3.35 3.10 2.84 2.67 2.45 2.42 2.33
2.26 2.24 2.20 2.16 2.20 2.33 2.41 2.54 2.74 2.94 3.21 3.51 4.05 4.56 4.99 5.00 5.20];
fb5=[6.50 6.55 6.60 6.65 6.70 6.75 6.80 6.85 6.90 6.95 7.00 7.05 7.10 7.15 7.20 7.25 7.30
7.35 7.40 7.45 7.50 7.55 7.60 7.65 7.70 7.75 7.80 7.85 7.90 7.95 8.00];
fb5=fb5*1.0e6;
ab5=[5.002 4.969 4.933 4.986 5.037 5.096 4.956 4.856 4.834 4.715 4.601 4.503 4.326
4.239 3.714 3.674 3.404 3.444 3.175 3.355 3.334 3.346 3.278 3.333 3.484 3.593 3.903
4.119 4.648 5.251 5.338];
%fb6=[4.10 4.15 4.20 4.25 4.30 4.35 4.40 4.45 4.50 4.55 4.60 4.65 4.70 4.75 4.80 4.85
4.90 4.95 5.00];
%fb6=fb6*1.0e6;
%ab6=[2.899 2.994 3.096 3.058 3.029 3.051 3.061 3.222 3.301 3.253 3.328 3.311 3.278
3.452 3.457 3.409 3.465 3.427 3.371];
fb7=[3.50 3.55 3.60 3.65 3.75 3.80 3.85 3.90 3.95 4.00 4.05 4.310 4.15 4.20 4.25 4.30
4.35 4.40 4.45 4.50];
fb7=fb7*1.0e6;
ab7=[0.4217 0.5237 0.6217 0.7975 1.337 1.542 1.948 2.389 3.085 3.918 4.075 4.168
4.478 4.398 4.225 4.418 4.566 4.301 4.478 4.656];

%Plot Results
%loglog(fp5,asp5,'ro')
%hold on
loglog(f1,as1,'b+')
hold on

```

```

loglog(f2,as2,'g+')
hold on
%loglog(f5r,as5r,'r-')
%hold on
loglog(f5,as5,'b+')
hold on
%loglog(f7,as7,'w+')
%hold on
%loglog(f10,as10,'y+')
%hold on
loglog(ff,af,'r-')
hold on
%loglog(fb,ab,'g*')
%hold on
%loglog(fb2,ab2,'g*')
%hold on
loglog(fb3,ab3,'g*')
hold on
loglog(fb4,ab4,'g*')
hold on
loglog(fb5,ab5,'g*')
hold on
%loglog(fb6,ab6,'g*')
hold on
loglog(fb7,ab7,'ro')
hold on
axis([1.0e5 2.0e7 1.0e-3 1.0e1])
title('Attenuation Results--5% polystyrene in 2" cell ')
xlabel('Frequency (Hz)')
ylabel('Attenuation (Np/cm)')
%loglog(f10r,as10r,'ro')
hold on

```

\*\*\*\*\*END OF STYRENE5.M\*\*\*\*\*

```

%Program to calculate the mean and standard deviation of
%the size measurements made on bubbles(generated both by
%aerator stone and electrolysis)using the video imaging systems.
%These measurements are then used to calculate a size distribution.
% Program is called " bublsize.m"

```

```

%Enter the aerator bubble measurements as arrays (bubble stream data)

```

```

daerstrm=[179 189 171 183 154 156 150 157 558 558 550 552 414 427 410 419 452 454
451 441 228 228 221 224 25 27 26 25 196 201 183 190 588 603 580 584 134 141 137
125 213 213 210 216 199 204 194 196];
maerstrm=mean(daerstrm);
sigaerstrm=std(daerstrm,1);

```

```

%data for aerator bubbles mixed
daermix=[378 381 373 375 51 53 50 45 140 147 138 150 162 168 160 163 175 173 174
180 204 199 192 201 166 169 149 161 171 161 159 168 164 156 155 59 171 164 166 166
106 113 101 102 164 166 160 157];
maermix=mean(daermix)
sigaermix=std(daermix,1)

```

```

%Enter the electrolysis bubble measurements as arrays (bubble stream data)
delestrm=[54 58 52 52 60 58 63 63 34 39 40 36 36 34 35 34 34 36 36 40 17 19 21 23 56
56 58 50 36 41 36 38 28 32 32 29 49 47 52 48 56 52 53 53 45 45 47 49 49 52 52 49 64 67
68 66 67 71 70 66 26 30 32 32 54 60 55 57 34 36 39 35];
melestrm=mean(delestrm);
sigelestrm=std(delestrm,1);

```

```

%Data for electrolysis mixed in the cell
delemix=[32 30 33 33 85 85 86 89 32 30 38 33 83 83 88 82 41 41 43 43 28 24 27 27 38
38 40 40 68 68 65 62 24 26 28 26 43 45 48 46 94 90 97 90 64 64 67 64 45 47 47 47 32 36
35 33 53 51 50 51 56 53 51 52 26 26 24 24 49 49 47 49 120 118 121 118 43 43 44 42 36
34 40 35 73 75 70 71 66 71 74 68 38 36 36 33 71 68 68 71 36 34 37 41 61 61 61 62 61 65
63 66 30 30 31 29 30 26 27 29 77 81 79 79 109 103 109 105 61 57 61 57 107 111 107
107 57 57 61 61 20 26 24 24 87 85 88 87 40 40 41 39 57 57 55 52 32 32 36 34 46 48 50
44 69 65 69 70 26 24 27 25 46 46 46 46 28 30 31 32 53 53 57 52 44 40 43 44 71 73 69 70
87 89 90 93 55 55 47 52 46 42 40 37 48 44 48 44 61 61 59 59 40 38 41 38 34 34 38 36 34
34 33 33 75 73 67 73];
melemix=mean(delemix)
sigelemix=std(delemix,1)

```

```

%delemix2=[61 61 61 62 61 65 63 66 30 30 31 29 30 26 27 29 77 81 79 79 109 103 109
105 61 57 61 57 107 111 107 107 57 57 61 61 20 26 24 24 87 85 88 87 40 40 41 39 57 57
55 52 32 32 36 34 46 48 50 44 69 65 69 70 26 24 27 25 46 46 46 46 28 30 31 32 53 53 57
52 44 40 43 44 71 73 69 70 87 89 90 93 55 55 47 52 46 42 40 37 48 44 48 44 61 61 59 59
40 38 41 38 34 34 38 36 34 34 33 33 75 73 67 73];
%melemix2=mean(delemix2)
%sigelemix2=std(delemix2,1)

```

```

%Calculate Bubble Size distribution
%Set up "bins" such that all bubbles in a bin are within 10 micron of bin diameter
rad=[0 10 20 30 40 50 60 70 80 90];
nrad=[0 0.1198 0.4101 0.2581 0.1429 0.04608 0.02304 0 0 0 ];

```

```
%Plot results
plot(rad, nrad, '-.')
ylabel('number fraction of bubbles')
xlabel('radius (micron)')
axis([0 100 0 0.5])
```

```
***** END OF BUBLSIZE.M*****
```

## **Appendix D: Experimental Parameter Series Coding**

The attenuation data presented in this study are obtained using a number of different combinations of transducers, mixing vessels, data acquisition methods, and slurry types. It is not obvious, upon examination of a given set of attenuation data, that it may have been collected from a slurry placed in more than one vessel (different acoustic pathlengths) and interrogated by more than one set of transducers. Therefore, a coding system is established to facilitate the acquisition of this information for every experimentally obtained set of data in this work. Each experimental figure has an experimental parameter number at the end of the figure caption. The experimental code has the following format:

E (I)(II)(III)(IV).

All codes begin with the letter “E” (for Experimental Parameter Series) followed by four digits, shown above by the Roman numerals I through IV. Each Roman numeral refers to an experimental set up parameter category shown in Tables D1 to D4.. Each category in Tables D1 through D4 has all the combinations of that parameter used in this study marked by a specific Arabic numeral. Thus the sequence of Arabic numerals following the “E” in the experimental code gives the pertinent information about the mixing vessels, transducers, etc. employed in obtaining that data set.

<u>Category I</u> -----	<u>Transducer Combinations</u>
1 -----	0.5 MHz, 1.0 MHz, 2.25 MHz, 5.0 MHz, 7.5 MHz, and 10.0 MHz
2 -----	1.0 MHz, 2.25 MHz, 5.0 MHz, 7.5 MHz, and 10.0 MHz
3 -----	1.0 MHz, 2.25 MHz, 5.0 MHz
4 -----	1.0 MHz, 2.25 MHz
5 -----	1.0 MHz, 2.25 MHz, 5.0 MHz, 7.5 MHz
6 -----	2.25 MHz, 5.0 MHz

Table D.1: Transducer combinations employed to obtain attenuation data in the various slurries investigated in this study.

<u>Category II</u> -----	<u>Experimental Method Combinations</u>
1 -----	Toneburst Method
2 -----	Pulse/FFT Method
3 -----	Both Techniques

Table D.2: Experimental method combinations employed to obtain attenuation data in the various slurries investigated in this study.

<u>Category III</u> -----	<u>Mixing Vessel/Test Cell Combinations</u>
1 -----	½" (1.27 cm) Plexiglas Test Cell
2 -----	1" (2.54 cm) Plexiglas Test Cell
3 -----	2" (5.08 cm) Plexiglas Test Cell
4 -----	4" (10.2 cm) Plexiglas Test Cell
5 -----	½" and 1" Plexiglas Test Cells

6	----- 1" and 2" Plexiglas Test Cells
7	----- ½", 1", and 2" Plexiglas Test Cells
8	----- ½" and 4" Plexiglas Test Cells
9	----- 4" and 1" Plexiglas Test Cells
0	----- 1.6 L PVC Mixing Vessel

Table D.3: Experimental mixing vessel/test cell combinations employed to obtain attenuation data in the various slurries investigated in this study.

	<u>Category IV</u> ----- <u>Slurries Investigated</u>
1	----- Soda-Lime Glass Beads (small beads) in Water
2	----- Potter's Beads in Glycerin/Water
3	----- Polystyrene Beads in Water

Table D.4: Various slurries investigated in this study.

An example of the interpretation of this coding system could be in the case shown in Figure 4.2, where we have a set of data labeled as E2363. This code implies the Experimental set up where the 1.0, 2.25, 5.0, 7.5, and 10.0 MHz transducers are used (Table D.1, item #2) in both the Toneburst and Pulse/FFT techniques (Table D.2, item #3) to obtain attenuation data in the 1" and 2" Plexiglas test cells (Table D.3, item #6) for a slurry of polystyrene beads in water (Table D.4, item #3). This coding system can be used to determine the experimental parameters relevant to each data set shown in this work.

## Appendix E: Discussion of Transducer Bandwidth

A parameter which is often discussed in reference to a given ultrasonic transducer is the transducer bandwidth. The bandwidth is a term which describes the frequency range over which a given transducer will function effectively. It is usually referred to as the “- 6 dB Bandwidth” and is described in terms of a percentage of the “peak frequency” of the transducer. The peak frequency is the frequency at which the FFT frequency spectrum of a received pulse (transducer response) displays a maximum. A signal which -6 dB from the peak frequency signal has one half of the peak frequency amplitude. As the transducer response is usually a bell shaped curve, there will be two frequencies which are -6 dB from the peak frequency. One frequency is greater than the center frequency, and one is less than the center frequency. The -6 dB bandwidth is the difference between those two frequencies divided by the center frequency, times 100 %. That is

$$\text{- 6 dB Bandwidth} = \frac{f_{-6\text{dB}}^+ - f_{-6\text{dB}}^-}{f_c} \times 100\%, \quad (\text{E.1})$$

where  $f_{-6\text{dB}}^+$  and  $f_{-6\text{dB}}^-$  are the frequencies at -6 dB from the center frequency which are greater and less than the center frequency, respectively, and  $f_c$  is the transducer center frequency. For example, a 0.50 MHz transducer with a reported center frequency of 0.457 MHz and -6 dB frequencies of 0.61 MHz and 0.305 MHz will have a bandwidth of 66.7 %.

## Notation

### Latin Characters:

<b>A</b>	=	Vector velocity potential, $m^2/s$
<b>a</b>	=	General vector quantity
<b>A</b>	=	Magnitude or scattering coefficient
<b>B</b>	=	Magnitude or scattering coefficient
<b>C</b>	=	Magnitude or scattering coefficient
<b><math>C_p</math></b>	=	Heat capacity at constant pressure, $J/gK$
<b><math>C_v</math></b>	=	Heat capacity at constant volume, $J/gK$
<b>c</b>	=	Sound speed, $m/s$
<b>d</b>	=	Deviatoric stress, Pa or path length, cm
<b>e</b>	=	Base of natural logarithm = 2.718
<b>f</b>	=	Transducer frequency, MHz
<b>g</b>	=	Indicator function
<b>h</b>	=	Spherical Hankel Function
<b>i</b>	=	$\sqrt{-1}$
<b>j</b>	=	$\sqrt{-1}$ or Spherical Bessel Function of First Kind
<b>k</b>	=	Wavenumber, $cm^{-1}$
<b>k</b>	=	Vector wavenumber, $cm^{-1}$
<b>N</b>	=	Total number of particles or bubbles
<b>n</b>	=	Number of bubbles per unit volume
<b>P</b>	=	Probability Density or Legendre Polynomial
<b>q</b>	=	Heat flux, $J/m^2s$
<b>R</b>	=	Bubble radius, cm
<b>r</b>	=	Position vector, cm, m
<b>r</b>	=	Bubble or particle radius or position, cm
<b>S</b>	=	Structure factor
<b>T</b>	=	Temperature, K
<b>t</b>	=	Time, s
<b>u,u</b>	=	Velocity, $m/s$
<b>V</b>	=	Control volume, $cm^3, m^3s$
<b>v</b>	=	Velocity, $m/s$
<b>v</b>	=	Attenuation, $cm^{-1}$
<b>x</b>	=	Position coordinate, cm, m
<b>x,y</b>	=	Position coordinate, cm, m

### Greek Characters:

$\alpha$	= Attenuation coefficient, $\text{cm}^{-1}$
$\beta$	= Bubble volume fraction or thermal expansion coefficient, $1/\text{K}$
$\gamma$	= Ratio of specific heats = $C_p / C_v$
$\varepsilon$	= Error parameter
$\delta$	= Deviatoric stress, Pa or damping coefficient or Dirac delta or Kronecker delta
$\eta$	= Parameter
$\theta$	= Radial angle, rad
$\lambda$	= Parameter or Lamè constant
$\mu$	= Viscosity, kg/ms or Lamè constant
$\rho$	= Density, $\text{g}/\text{cm}^3$
$\pi$	= 3.14159
$\Phi$	= Scalar velocity potential, $\text{m}^2/\text{s}$
$\varphi$	= Azimuthal angle, rad
$\phi$	= Solids volume fraction or scalar velocity potential, $\text{m}^2/\text{s}$
$\omega$	= Angular Frequency, MHz
$\sigma$	= Stress tensor, Pa or surface tension, dyn/cm
$\tau$	= Thermal Conductivity, $\text{J}/\text{Kcms}$

### Superscripts and Subscripts:

<i>c</i>	= Compressional
<i>H<sub>2</sub>O</i>	= Water phase
<i>i,j</i>	= Indicinal subscripts
<i>e</i>	= From the energy equation
<i>eff</i>	= Effective value
<i>EM</i>	= Effective Medium
<i>G</i>	= Gas phase
<i>L</i>	= Liquid phase
<i>meas</i>	= Measured value
<i>P</i>	= Particle
<i>s</i>	= solid or shear
<i>t</i>	= thermal
<i>true</i>	= True value
<i>slurry</i>	= slurry
<i>solid</i>	= solid phase
0	= Initial or equilibrium value
*	= Superscript implying dimensionless quantity
~	= Superscript implying quantity evaluated inside a particle.

## Vita

**NAME OF AUTHOR:** Michael Anthony Norato

**DATE OF BIRTH:** January 25, 1969

**PLACE OF BIRTH:** Philadelphia, Pennsylvania, USA

### **GRADUATE AND UNDERGRADUATE SCHOOLS ATTENDED:**

Bachelor of Science, 1991;

Department of Chemical Engineering and Materials Science, Syracuse University,  
Syracuse, New York, USA.

Master of Science, 1994;

Department of Chemical Engineering and Materials Science, Syracuse University,  
Syracuse, New York, USA.

### **PROFESSIONAL EXPERIENCE:**

Department of Chemical Engineering and Materials Science, Syracuse University:  
Teaching Assistant, 1991, 1995, 1996, & 1997.

Research Assistant, 1991-Present.

Associated Western Universities/Battelle Pacific Northwest National Laboratory:  
Graduate Laboratory Fellow, 1996.